UCID- 20884

HOTSPUR:
GAMMA RAY EMISSION FROM SPHERES PULSED WITH D-T NEUTRONS

I. Calibration of Improved NE213 Detector Assembly
II. Comparison of TART/SANDYL Electron Recoil Spectra to Experiment; Preliminary Results

E. Goldberg
L.F. Hansen
T.T. Komoto
B.A. Pohl

September 1986

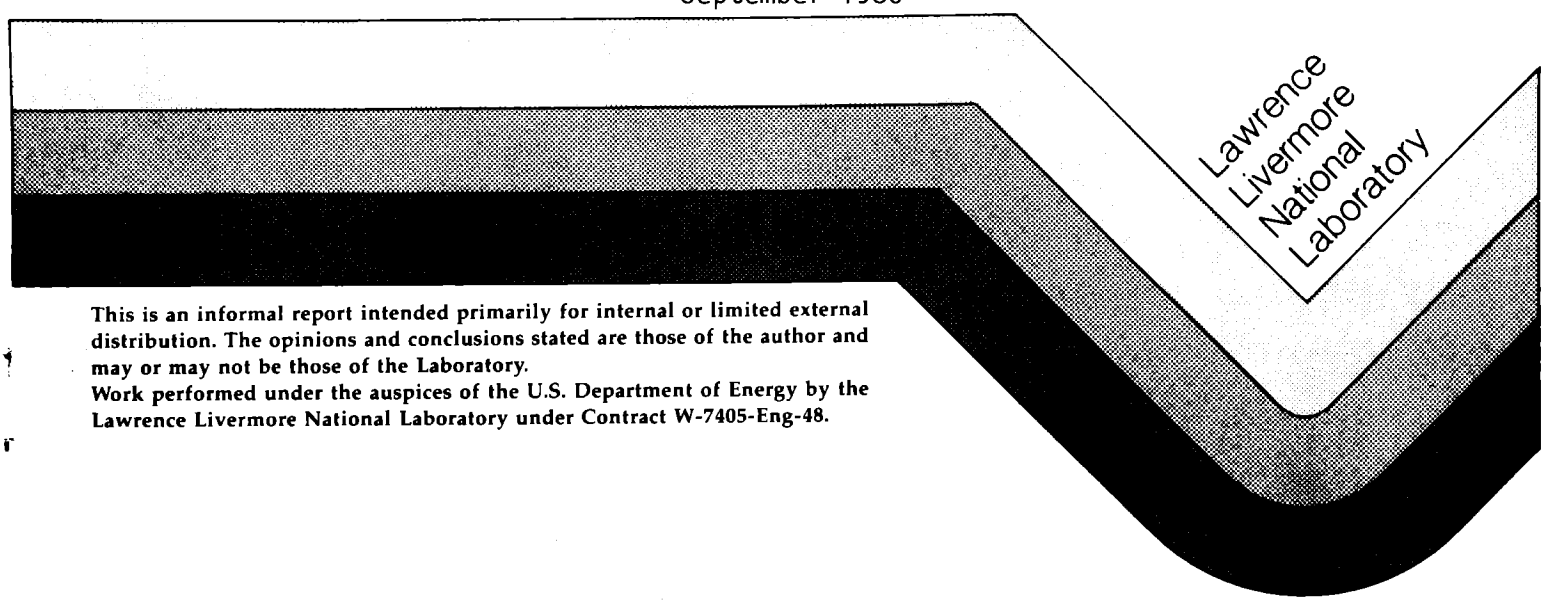

Work performed under the auspices of the U.S. Department of Energy by the Lawrence Livermore National Laboratory under Contract W-7405-Eng-48.

Printed in the United States of America
Available from
National Technical Information Service
U.S. Department of Commerce
5285 Port Royal Road
Springfield, VA 22161

Price Code	Page Range
A01	Microfiche
Papercopy Prices	
A02	001 - 050
A03	051 - 100
A04	101 - 200
A05	201 - 300
A06	301 - 400
A07	401 - 500
A08	501 - 600
A09	601

HOTSPUR:
GAMMA RAY EMISSION FROM SPHERES PULSED WITH D-T NEUTRONS

I. Calibration of Improved NE213 Detector Assembly

II. Comparison of TART/SANDYL Electron Recoil Spectra to Experiment; Preliminary Results

E. Goldberg
L.F. Hansen
T.T. Komoto
B.A. Pohl

University of California, Lawrence Livermore National Laboratory
Livermore, California 94550

I. DETECTOR CALIBRATION

Our first attempt to calibrate the NE213 scintillator detector was discussed in detail in the memorandum of February 28, 1986.[1] The pulse height as a function of electron energy became progressively nonlinear as the electron energy exceeded 2.75 MeV. Experiments were then performed in which spheres of various materials were pulsed with DT neutrons and the emergent neutrons and gamma rays registered signals on the NE213 detector. We found that the detector nonlinearity seriously interferred with our efforts to compare the TART/SANDYL - generated electron recoil spectra to the experimental counterpart for those experiments having gamma leakage spectra with significant components above ~ 3 MeV. Consequently, following Thorngate's recommendation,[2] we modified the detector system so that the pulse height would be linear with electron energy over the full range of interest.[1] Since our experiments included water, this implied gamma rays up to 7.1 MeV.

1. Hotspur memorandum of February 28, 1986; E. Goldberg, L.F. Hansen, B.A. Pohl.
2. UCID 20644 (to be released), J.W. Thorngate, "Improvements in the Apparatus and Procedures for an Organic Scintillator Used as Fast Neutron Spectra Meter for Radiation Protection Applications."

Correlation of Pulse Height with Electron Energy

Experiments were performed on April 21, 1986, to calibrate the new NE213 detector assembly. As in the earlier exercise, an aluminum disc was irradiated at RTNS-II to generate a ^{24}Na source. The ^{22}Na, ^{137}Cs, and ^{60}Co sources were independently calibrated. The ^{22}Na source first used in this series, mounted on a thin foil, was suspect and so we repeated on May 19 the calibration with another ^{22}Na source. This issue, to be discussed in greater detail below, involved the possibility of recoil of positrons from the source material and annihilation at a distant point.

Conversion Curve

Table I lists the characteristics of the sources used to generate the conversion curve (i.e., channel number versus E(electron)). The source strength (S_{run}) listed is equal to the number of photons emitted during the calibration exposure period, Δt.

a. ^{24}Na

The ^{24}Na source was produced by exposing a 0.0127-cm thick 1.27-cm diam. aluminum disk to D-T neutrons made at the RTNS-II facility, and calibrating it at the LLNL Nuclear Chemistry facility. The procedure outlined in the February 28 memo (Ref. 1) was closely followed. Comparison of experiment to SANDYL calculations demonstrated that the Compton cutoff energy coincided with that point of the electron recoil spectrum where the count rate fell to 80% of the Compton peak. This correlation allows us to construct an (electron energy) versus (channel number) relationship independent of SANDYL calculations. Figure 1 illustrates the ^{24}Na data gathered on April 21. We list in Table II the channel number corresponding to the (80% of peak)-value. The second entry for ^{24}Na represents the double-escape peak (i.e., 2.754-1.022, or 1.732 MeV).

TABLE I. GAMMA RAY SOURCE CHARACTERISTICS

SOURCE	SOURCE NO.	E_γ (MeV)	$E^a_{c.c.}$	$T_{1/2}$	Δt^c (min)	S_{run} (photons)
^{24}Na	-	1.369 2.754	1.154 2.520	15.00 h	66.0	1.27×10^9
^{22}Na	1x743	0.511 1.275	0.341 1.061	950.4 d	60.0	1.61×10^{9d}
^{137}Cs	700	0.662	0.477	30.17 y	20.31	1.14×10^{9e}
^{60}Co	225	1.173 1.332	0.963 1.118	5.271 y	17.0	1.06×10^8
PuBe (^{12}C) [b]	-	4.439	4.197	-	66.0	-
(^{16}O) [b]		6.130 6.919 7.117	5.885 6.672 6.870	-	-	-

[a] $E_{c.c.} \equiv$ Compton Cutoff Energy $= E_\gamma \; / \; (\frac{.2555}{E_\gamma} + 1)$

[b] (n,n')

[c] Calibration run

[d] For each disintegration, 1.808 photons at 0.511 MeV, 1.00 photons at 1.275 MeV

[e] For each disintegration, 0.8505 photons

b. ^{22}Na

Figure 2 illustrates the electron recoil distribution for an ^{22}Na source (#7599-2). We extract the channel number - electron energy correlation from this data since it was recorded on April 21, when the electronics system gain was constant for all the measurements on that day. (Below, we will refer to another ^{22}Na exposure when we extract the absolute calibration of the detector based on a more reliable source characterization.)

Table II lists the ^{22}Na correlation for the two Compton cutoff values.

c. ^{137}Cs

The spectrum for ^{137}Cs is very simple since only the 0.662 MeV gamma ray contributes to the signal. Figure 3 illustrates the data. Table II summarizes the correlation of electron energy to channel number.

d. ^{60}Co

For each disintegration of ^{60}Co, two gamma rays, one at 1.17 and one at 1.33 MeV, are emitted. The distribution is shown in Fig. 4. The resolution of the measurements does not allow a clean separation of the peaks in the recoil spectrum, so in Table II we entered only the channel number corresponding to the 1.17 MeV gamma ray.

e. $^{12}C^*$

We used a Pu-Be source to generate 4.439 MeV gamma rays from the Be $(\alpha,n)^{12}C^*$ reaction. The first excited state of ^{12}C is at 4.439 MeV and the above reaction insures sufficient energy to form $^{12}C^*$. The correlations are summarized in Table II.

TABLE II. CHANNEL NUMBER vs ELECTRON RECOIL ENERGY IN NE213 DECTECTOR

DATE	SOURCE	E (Electron) MeV	CHANNEL NO.[a]	COMPTON EDGE	DOUBLE ESCAPE PEAK	CORRECTED CHANNEL NO.
4/21	^{22}Na	0.341	38	X		
		1.061	124	X		
4/21	^{24}Na	1.154	137	X		
		1.732	205		X	
		2.520	301	X		
4/21	^{137}Cs	0.478	53.7	X		
4/21	^{60}Co	0.963	116	X		
4/21	$^{12}C^*$	3.417	405		X	
		4.197	498			
6/3	$^{16}O^*$	5.108	675		X	609
		5.885	780	X		703
		6.754	870	X		785

a. At 80% of peak value.

f. $^{16}O^*$

When H_2O is irradiated with D-T neutrons, energetic gamma-ray lines are generated from excitation of ^{16}O. Its first excited state is at 6.13 MeV and de-excitation gamma rays from this state enabled us to extend the correlation range up to this energy.

Figure 7 of the February 28 note (Ref. 1) is similar to the findings of June 3, to be discussed in detail later. The prominent features provide three correlation pairs, summarized in Table II. A correction is necessary since the gain of the multi-channel analyzer had been altered for the June 3 run. The correction employed was the ratio of the channel numbers for the higher ^{22}Na peak. For the April 21 run, it was 119.5 while for the June 3 run it was 132.5. This ratio was applied to give the corrected values listed in Table II.

g. Revised Conversion Curve

The contents of Table II are summarized in Figs. 5A and 5B. The points are well fit by the expression:

$$\frac{E\ (\text{Electron}) - .026}{\text{Channel No.}} = 0.00829 \qquad (1)$$

If one does not include the highest energy point, we find that the standard deviation of the individual channel numbers about the curve defined above is 1%. The quality of the data represented by the highest point is questionable, since it depends on knowledge of the relative strengths of the 6.9- and 7.1 MeV lines generated by ^{16}O excitation, with respect to the 6.13 MeV line. In the following analyses, we will use the expression as given, when the Compton peak of the upper ^{22}Na line is at Channel 124. For circumstances where that peak is shifted, we scale the RHS linearly.

NE213 Detector Calibration

The absolute calibration of the NE213 detector was done with ^{22}Na, ^{24}Na, ^{60}Co, and ^{137}Cs calibrated gamma ray sources. Careful comparison of this data to SANDYL calculations provided us with a means of correcting the SANDLY predictions when applied to the experiments which incorporated a D-T neutron source centrally located within a spherical assembly.

a. ^{22}Na

When a ^{22}Na source was employed, the results of the SANDYL calculations were found to underpredict the sensitivity of the NE213 detector (Fig. 2). This was noteworthy since the other comparisons were all in the other direction. After some thought, the possibility was raised that the ^{22}Na source used on April 21, 1986, (#7599-2) was not properly configured. A properly designed source should release for each disintegration 1.00 photons at 1.275 MeV and 1.808 photons at 0.551 MeV at a well-defined position in space (ref. Table of Isotopes, Seventh Ed., Lederer and Shirley). The ^{22}Na decays via positron emission 90.5% of the time and the remainder goes via electron capture. The 1.275 MeV line corresponds to de-excitation of ^{22}Ne. The positron end-point energy is 0.5457 MeV (Lederer and Shirley) which leads to a likelihood that a significant portion of the positrons can escape from the 0.53 mm-thick source foil.

To clear up this issue, additional experiments were performed on May 19, 1986, to highlight the differences in responses of the NE213 detector to different ^{22}Na sources. A calibrated source of more conventional design (#1X743), 2.31 mm thick, was first used with no covering and then was sandwiched between 0.6-mm-thick aluminum foils. Finally, we repeated the experiment using the thin source (#7599-2).

The two measurements using Source No. 1X743 gave very similar results. Figure 6 illustrates the findings with a source covered by the aluminum foils. The experimental points

have been corrected for background as have the findings for ^{24}Na, ^{60}Co, and ^{137}Cs discussed below. The pulse height analyzer gain for the May 19 experiments was slightly higher than that of April 21. The conversion of SANDYL electron energy spectra to channel units is given by the expression:

$$E\ (\text{Electron}) - .026 = 0.00805 \times (\text{Channel Number}).$$

Here we see over the lower Compton peak that the SANDYL calculations exceed experiment by ~7%. Over the higher peak, smoothed by folding in a normal distribution ($\sigma/\bar{E}$ ~.025) calculations, exceed experiment by ~3%. This differs markedly from the results of Fig. 2 thus reinforcing the belief that positron escape from the source foil #7599-2, and annihilation closer to the detector, leads to a ratio of calculation to experiment less than unity.

b. ^{24}Na

Figure 1 illustrates the experimental electron recoil distribution for the ^{24}Na source. The SANDYL results based on the relationship of Fig. 5, have been smoothed with a normal distribution where $\sigma/\bar{E}$ ~.025. We see, by integration under the appropriate segments of the distribution, the (SANDYL/experiment) ratio to be 1.04 (lower peak), 1.00 (double-escape peak), and 1.02 (upper peak).

c. ^{137}Cs

In the note of February 28 (Ref 1) we found that the SANDYL distribution, when smoothed by a function with $\sigma/\bar{E}$ ~.05, reproduced the shape of the experimental data for ^{137}Cs, but the calculated Compton peak exceeded experiment by 12%. Here also, as we see in Fig. 3, SANDYL results consistently exceed experiment by ~12%.

d. ^{60}Co

Figure 4 compares SANDYL findings, based on a smoothing function, $\sigma/\bar{E}$ ~0.025, and Fig. 5's relations, to the experimental data of April 21, 1986. On the average, calculation exceeds experiment by 4%. If we energy-weight, this drops slightly to 3%, in good agreement with the findings of Ref. 1.

e. Summary of Calibration Results

From the preceding considerations, we can extract an average correction factor to normalize SANDYL calculations with respect to the calibration experiments. We find

$$(\text{SANDYL/Experiment}) = 1.05 \pm 0.04$$

The ratio appears to be electron recoil energy-dependent, with the larger value (~1.095) at lower energies. We will, since the variation is essentially within the uncertainty, employ a constant correction factor to simplify the analysis.

All of the SANDYL calculations were performed with the NE213 density at 0.884 g/cm^3, a value used several years ago. The value found in the published literature and supplier's specification is 0.874. If we had used the latter, the correction factor would have dropped to 1.04.

In subsequent analysis of the pulsed sphere experiments, we will reduce the SANDYL-derived electron recoil spectra by 5% to normalize to the calibration experiments.

II. NEUTRON-INDUCED GAMMA RAYS; PRELIMINARY RESULTS

The neutron time-of-flight technique is well suited to gamma-ray and neutron spectral measurements. Since the gamma rays travel at the velocity of light, always greater than that of any neutrons, time discrimination may be employed to suppress background neutron-induced radiation. In the present series, the experimental configurations were designed to facilitate background suppression.

The distance between the D-T source and center of the NE213 detector was 852 cm. The neutron source was in one room while the detector was in another, separated by a concrete wall. An iron collimator 197 cm long with a 20.2 cm inner diameter and surrounded by a water jacket, was positioned with its axis horizontal and colinear with the source and detector direction. The tritium target was 512 cm from the collimator face while the detector center was 143 cm from the exit face. Spheres of various materials were restricted in radius to $\leq$15 cm so that the collimator would not obstruct the path of the gamma rays from the sphere to the detector. A time window of 67 ns, centered on the gamma peak, was chosen for the gammas.

a. Procedure for Calculation of Gamma-Ray Output and Electron Recoil Spectra

The calculations pertaining to neutron-induced gamma rays are more involved than those relating to neutron spectra. The neutron time-of-flight analysis basically normalizes the neutron leakage spectra to the unattenuated (i.e., sphere-out) spectrum, whereas the gamma-ray analysis requires knowledge of the absolute neutron source strength and absolute calibration of the gamma-ray dectector.

For each experiment, the neutron strength was monitored by recording the alpha counts accumulated by the associated particle detector and also the signal from a proton recoil counter (PRCB) (i.e., one of two counters normally available). During the course

of the measurements, many "blank" or sphere-out runs were alternated with sphere-in runs to assure stability of the instrumentation.

The PRCB detector had been calibrated earlier[3] with respect to the $^{27}Al(n,\alpha)^{24}Na$ reaction. The findings are summarized for that study:

Technique	Inferred Neutron Source Strength ($n \times 10^{-16}$)
$^{27}Al(n,\alpha)^{24}Na$	7.76 ± 0.11
PRC A	7.98 ± 0.40
PRC B	8.34 ± 0.42
PRC Av.	8.16 ± ~ 0.41

The conversion factor for PRCB is specified to be:[4]

$$5.55 \times 10^{7} \text{ n/ster./ct, } \Theta=0° \text{ and } R=100 \text{ cm.}$$

Normalizing to the $^{27}Al(n,\alpha)^{24}Na$ cross section, this reduces to:

$$5.55 \times 10^{7} \times \frac{7.76}{8.34} = 5.16 \times 10^{7},$$

which implies an adjustment of ~7%. If we refer to a typical blank run (No. 13, 6/4/86), the PRCB/α count ratio, where the PRCB is positioned at ~45° and is 50 cm from the source, is 0.129. The alpha particle detector is then found to have the calibration factor:

$$0.129 \times \frac{5.16 \times 10^{7}}{4} = 1.66 \times 10^{6} \text{ n/ster.}\alpha \text{ count}$$

3. UCRL-92817, Rev. 1, D.W. Kneff, B.M. Oliver, E. Goldberg, and R.A. Haight (3/10/86).

4. Private communication, Rex Booth.

which agrees well with the earlier value generally quoted of 1.64×10^6.[5] This somewhat circuitous route to the neutron strength is outlined since the PRCB response with a sphere in place is affected by the sphere material in an unknown way. We therefore periodically recalibrate the alpha detector each time we do a blank run. The neutron source strength is then simply:

$$(\text{alpha counts}) \frac{(\text{PRCB}/\alpha)_{\text{blank}}}{.129} \times 1.66 \times 10^6 \times \frac{4\pi}{1.06} \text{ (neutrons)},$$

where the slight anisotropy of the neutron source is taken into account.[6]

The TART code, on request, will accumulate the kinematic parameters for each particle which enters a specified zone. In the present study, we tallied these parameters for gamma rays and neutrons which entered a thin test zone, 879 cm from the source whose transverse boundary was defined by a cone of 30°-half angle.

To treat gamma rays, an edit code, XGAMEDIT, was written.[7] Input parameters established the maximum angle allowed for inclusion in the tally and maximum time of crossing the test surface. The angle restriction was based on the largest angle allowed for passage through the collimator, while the time restriction accounted for the TART zero time for the neutron source, the gamma-ray flight time, and half width of the time window, 67/2 ns. The angle restriction used throughout was ~15/852, or 0.018 radians based on the collimator constraint. Where the spherical radius of the sphere was significantly smaller than 15 cm, the use of the 15 cm value allowed the surrounding air to contribute to the signal.

5. Private communication, Luisa Hansen.
6. C. Wong, J.D. Anderson, P. Brown, L.F. Hansen, J.L. Kammerdiener, C.M. Logan, and B.A. Pohl, "Livermore Pulsed Sphere Program, Program Summary through July 1971", UCRL-51114, Rev. 1, Lawrence Livermore Laboratory (1972).
7. E.F. Plechaty and T.T. Komoto, private communication.

The edited gamma-ray leakage spectrum from TART was then modified into equal probability bins for the SANDYL input, and SANDYL calculations were performed in which the photons were colinear and uniform over the face of the NE213 detector. To get the filtered gamma fluence (FGF), the tallied photons per neutron (TPN) (which is generated as the HTRTØ file by XGAMEDIT acting on TART output file, GCORDØ) are altered by the geometric factors.

$$FGF = \frac{TPN \times N}{.06699 \times 4\pi (\Delta Z)^2} \quad (\text{gamma rays/cm}^2)$$

where in the present series, ΔZ=852 cm, and 0.06699 is simply the fractional solid angle defined by $0° \leq \theta \leq 30°$.

Finally, using the gamma source probability table as SANDYL input, we generate the (counts/MeV/photon). To get the observable quantity, (counts/counter channel), the operation is straightforward:

$$\frac{\text{Counts}}{\text{Channel}} = \frac{\text{Counts}}{\text{MeV Photon}} \times (\text{Area of Detector, } A_D) \times FGF \times C.F.,$$

where C.F. is the conversion factor, i.e., (MeV/Channel), which was determined experimentally in the detector calibration study.

Summarizing, to get the calculated electron recoil spectrum for comparison to the gamma-ray induced signal from a D-T neutron pulsed sphere, we do the following:

1. Determine neutron strength from alpha particle counter.
2. From TART, find [γ fluence/neutron] via the XGAMEDIT code to generate HTRTØ file, the output gamma-ray spectrum, and TPN.
3. Construct from TART output gamma-ray spectrum the SANDYL input.
4. From SANDYL, generate (counts per channel).

For subsequent error analysis, it is useful to put this all together to find the overall conversion factor of the SANDYL-generated ($\frac{\text{cts}}{\text{MeV photon}}$) to the experimental ($\frac{\text{cts}}{\text{channel}}$):

$$\left(\frac{\text{cts}}{\text{channel}}\right) = \left(\frac{\text{cts}}{\text{MeV photon}}\right) \times A_D \times 1.29\times10^{7} \times \left(\frac{\text{PRCB}}{\alpha}\right)_{\text{Blank}} \times \alpha_i$$

$$\times \frac{\text{TPN}}{0.06699} \times \frac{1}{4\pi(\Delta Z)^2} \times \text{C.F.}\left(\frac{\text{channels}}{\text{MeV}}\right) \times \frac{1}{1.05}$$

The last term is the gamma-ray calibration correction.

b. Experimental Data and Comparison to TART/SANDYL

A large number of spherical assemblies were investigated in the series performed on June 2-6, 1986. Of these, we have analyzed spheres of tungsten, graphite, iron, water in a glass vessel, ^{238}U, ^{232}Th, gold, aluminum, copper, and tantalum, to date. Table III summarizes many of the parameters employed in the analysis. Also included is the blank run (Run No. 13) which we first discuss.

1. Blank (Sphere Out) Experiment

Although the neutron source at RTNS-I has been designed with minimum mass as a goal, the gamma rays generated by the D-T neutrons acting upon the assembly cannot be ignored. The tungsten target backing, nominally 0.76 mm thick, is a major contributor in a blank run because of its close proximity to the T target. Also, the air plays an important role when irradiated by fast neutrons.

The procedure outlined above to generate the electron recoil spectrum in the NE213 detector was applied to a typical blank run (#13, 6/4/86). TART and SANDYL inputs are listed in Appendix A. The TART gamma-ray output was edited with the constraint that the gamma rays arrive at a time not later than 33.5 ns after the gamma peak, in accordance with the electronic gate setting. Further, photons were accepted only if their angular deviation on exit over a distance of 852 cm was less than that resulting from a transverse dislacement of 15 cm at the source. (This is equivalent to the effect of the

TABLE III. SUMMARY OF PARAMETERS

Material	Outer Radius (cm)	$\rho\Delta Z$ (g/cm^2)	N x 10^{-12}	$\left(\frac{PRCB}{\alpha}\right)_{Bl.}$	α x 10^{-5}	TPN	TT12	C.F. (MeV/ch.) x 10^3
Tungsten	10.36	49.0	5.61	0.1315	2.79	0.01001	0.0124	7.516
Graphite	10.16	17.71	5.67	0.128	2.90	0.0153	0.0181	8.087
Iron (1)	4.46	31.3	4.90	0.129	2.49	0.0427	0.0476	7.516
Iron (2)	4.46	31.3	2.28	0.119	1.25	0.0427	0.0476	11.90
Water,empty	14.76	1.11[a]	3.46	0.131	1.72	0.00766	0.0104	7.516
Water,full	14.76	+13.36[b]	10.04	0.131	5.01	0.02145	0.0241	7.516
^{238}U	3.63	55.75	2.23	0.121	1.20	0.0143	0.0171	7.516
^{232}Th	5.76	61.6	4.61	0.121	2.49	0.0107	0.0131	7.516
Gold	6.21	120.0	5.57	0.131	2.78	0.00790	0.00968	7.516
Aluminum	8.94	22.4	2.52	0.119	1.38	0.05586	0.0587	11.90
Copper	4.00	32.9	4.42	0.121	2.39	0.03774	0.04289	7.516
Tantalum	3.40	51.1	4.48	0.121	2.42	0.01368	0.01631	7.516
Blank	0	0	2.08	0.129	1.07	0.00465	0.00733	7.516

[a] Glass

[b] H_2O (i.e., 13.36 g/cm^2 H_2O + 1.11 g/cm^2 pyrex)

collimator.) The gamma spectrum employed is listed in the SANDYL input in a handy format, corresponding to 32 equal probability bins.

Figure 7 compares experiment and calculation. The calculated points have been reduced by 5% to account for the gamma-ray calibration. The ordinate is in experimental units -- electron counts per channel -- while the abscissa is given in channel number to simplify the comparison.

Integration of the calculated points gives a gamma-ray energy leakage, assuming isotropic leakage, of 0.134 MeV per 14-MeV source neutron. If no angle or time constraint is applied, this value rises to 0.26 MeV per D-T neutron. The ratio of calculation to experiment is 0.93 ± 0.07 for electron energies ranging up to 5 MeV. At higher energies where there is large statistical uncertainty, the calculated counts per channel rises significantly above the experimental values. This will be seen below to be an artifact of the TART code description of gamma-ray spectra -- the upper energy limit of the uppermost gamma-ray energy bin appears to have been selected too high, in general, for the materials which contribute gamma rays in the blank runs.

Since the ratio is sufficiently close to unity, we will not attempt to correct for the discrepancy. We should expect, for spheres which are thick to D-T neutrons, to see the above discrepancy mitigated, since the gamma rays originating at the source will be attenuated by the sphere material.

Additional calculations demonstrated an ability to distinguish individual contributors to gamma-ray production. When in TART the tungsten backing was reduced from 0.76 mm to 0.51 mm, the electron counts per channel for channel numbers less than 260 (i.e., E(electron) $\leq$2 MeV) dropped by ~20%.

To further delineate the components of the gamma-ray background, a copper shadow bar of 5.08 cm diam. and 45.5 cm length was positioned along the source-detector axis to intercept any radiation originating in the source and moving

in a direct path to the detector. The bar upstream face was 1.0 m from the source. The detector signal was strongly attenuated. We found the signal to be ~7% of the blank run signal after normalization with respect to alpha particle counts, and the spectrum to be similar to that from the blank run. We believe that most of the shadow bar signal is due to interaction of D-T neutrons and source-generated gamma rays with the air. Several XGAMEDIT calculations were performed upon the TART edit to determine the effect of the choice of the limiting angle of acceptance. We found, for transverse selection distances of 2.54 cm and 15 cm, a difference of 5% of the blank signal. We may then infer that a negligible (i.e., $\leq$2%) amount of the blank signal arises in the deuteron beam pipe upstream of the source which is visible to the detector.

2. Tungsten Spherical Shell

In our initial attempt to investigate tungsten (January 28, 1986) we chose a spherical configuration with a 10.4-cm radius. It became clear that the gamma signal was strongly attenuated by self-absorption. This was substantiated by a series of simplified TART calculations, the results of which pointed to thicknesses between 1.3 and 2.5 cm, as well-suited to maximize the gamma-ray output signal. Accordingly, for the present exercise, we chose a set of tungsten metal shells (ρ=19.3 g/cc) with a 7.72 cm-inner radius and 10.36 cm-outer radius, and a median gap of 0.1 cm, for which $\rho\Delta R$=49.0 g/cm^2.

The D-T neutron source strength was 5.61×10^{12} n. TART calculations gave 0.0100 gamma rays per source neutron leaking across a surface with a 0-30° solid angle, at a distance of 852 cm from the source. Figure 8 compares the expeimental data with the TART/SANDYL-based calculated electron recoil spectrum which utilizes the experimentally-determined neutron source strength.

We find the calculated points to be 30-40% below experiment. The uncertainty attached to calculations (which includes the neutron source strength) is crudely estimated at 10%, so we see the discrepancy to be well above the uncertainty. The crossover of the curves at Channel No. 650 (equivalent to ~6 MeV electron energy) and divergence as energy increases is likely due to the representation in the cross-section tables. The uppermost equal probability bin extends up to 12 MeV gamma energy, leading to a curve not in accord with experiment.

3. Graphite

Chronologically, the graphite sphere was the first investigated in the June series. Its gamma-ray spectrum was expected to closely resemble the Pu-Be gamma-ray spectrum. Due to initial drift of the gain in the electronic circuits, the electron recoil spectra was not as expected. So we inferred the relationship of electron energy to channel number from the double-hump character of electron recoil spectrum attributed to the 4.439-MeV gamma ray arising from de-excitation of ^{12}C. Figure 9 shows that the goal was accomplished and further the (counts per channel) calculation agrees very well with experiment over the double hump. The SANDYL distribution was smoothed with a function in which $(\sigma/\bar{E})=0.04$. Below Channel 400 (E_ε~3.25 MeV) calculation is ~6% below experiment.

4. Iron

Prior TART calculations pointed to the need of a small sphere of iron to reduce gamma ray self-absorption, so a sphere with an outer radius of 4.46 cm was chosen. We investigated iron twice in the June series, the second run at reduced gain, to study more closely the gamma-ray high energy tail. Figures 10A and 10B illustrate the findings. For

electron energies below 1.0 MeV, agreement between experiment and calculation is good, whereas above 1.0 MeV the calculations exceed experimental data by ~20%.

5. H_2O-Filled Glass Spherical Flask

For this investigation, a glass vessel was fabricated[8] to provide us with a convenient container for the H_2O. A 29.5-cm diameter, 0.28-cm thick spherical Pyrex flask penetrated by a Pyrex test tube with a 0.20-cm-thick wall was first used empty and was then filled with water. Table III lists additional information. The transparent container proved to be very advantageous, facilitating alignment of the neutron source with the center of the vessel. The maximum H_2O areal density (along the test tube axis, which coincides with the beam axis), is 13.36 g/cm^2.

Figures 11 and 12 compare calculation to experiment for the empty and filled vessels, respectively. Large discrepancies are observed for the H_2O-filled vessel. For E_ε~4-5 MeV, calculated counts per channel exceed experiment by a factor of two. The present TART cross-section set is referenced back to 1973.[9]

6. ^{238}U

We see in Fig. 13 excellent agreement between calculation and experiment for a ^{238}U sphere of 3.63-cm radius. Above Channel No. 300 (i.e., E_ε~2.3 MeV) the two curves diverge. Again, this behavior is likely due to the data base format which exaggerates the importance of the choice of the upper limit of the uppermost gamma ray energy group (in this case, 12 MeV).

8. The vessel was kindly furnished by Mel Bishop (MFD Glassblowing Shop).
9. UCIR-718, R.C. Haight, S.T. Perkins, M.H. MacGregor, and R.J. Huntington, "Evaluation of Neutron Induced Gamma-Ray Production Cross Sections, Angular Distributions, and Spectra", August 16, 1973.

7. ^{232}Th

The results for a 5.757-cm radius ^{232}Th spherical assembly is illustrated in Fig. 14. There we see the ratio of calculated to experimental counts per channel to be 10-15% below unity for most channels below 260 (i.e., E_ε~2 MeV) and above that value the ratio rises to a factor of two and more. Recalling the empirical formalism of Howerton and Plechaty[10] which was drawn upon to generate the cross-section data base for ^{232}Th, where the gamma spectrum varied as $E_\gamma \exp(-RE_\gamma)$ with R an empirical constant, a slight increase in (R) is indicated if one continues to adhere to this formalism.

8. Gold

Figure 15 shows fairly good agreement for a 6.21-cm radius gold sphere, with trends similar to that for ^{232}Th. At lower electron energy, calculation is ~15% below experiment and, as electron energy increases, crossover occurs at E_e~1.85 MeV, and calculation rises ~15% above experiment at E_e~3 MeV. In this case again a slight increase in (R) is warranted.

9. Aluminum

For an 8.94-cm radius aluminum sphere, the calculated counts per channel is consistently 10-30% above experiment.. Viewing Fig. 16, considerable structure is apparent in the electron recoil spectrum as evidence of strong line structure in both experiment and calculation. A smoothing function was not employed with the calculated spectrum. If it were, the (calculated/experimental) ratio would be C/E~1.2.

10. Copper

The comparison of experiment to calculation for a 4.00-cm radius copper sphere in Fig. 17 shows the calculated counts per channel to vary within ±25% of the measurements over most of

10. R.J. Howerton and E.F. Plechaty, N.S.E. 32, 178 (1968)

the range of pulse heights. No prominent features are apparent in the distribution. We see better agreement between experiment and calculation for copper than for iron, illustrated in Figs. 10A and 10B.

11. Tantalum

Figure 18 summarizes the comparison of the experimentally determined electron recoil spectrum generated by a 3.40-cm radius tantalum sphere, and the TART/SANDYL calculation. The calculated values are seen to fall 20-30% below the measured values. The tungsten exercise also exhibited the same trend, with an even greater disparity. No prominent features are apparent in the experimental distribution. We see again evidence that the high energy tail is misrepresented in the TART calculation, leading to an overestimate of photons above ~5 MeV.

Comments

We submit the gamma-ray results of the pulsed sphere experiments performed on June 2-6, 1986, in preliminary form to initiate discussion on our findings. Clear discrepancies exist for some of the materials. We see TART to overpredict gamma-ray emission from a D-T neutron-pulsed tungsten spherical shell, and a tantalum sphere, while TART clearly overpredicts gamma emission from D-T neutron-pulsed water (i.e., ^{16}O) and aluminum.

Still ahead is a careful comparison of the neutron time-of-flight spectra to their respective electron recoil spectra and examination of the cross-section data base incorporated in TART. It would be logical, where discrepancies between calculation and experiment exist, to utilize other cross-section sets such as ENDF.

We also are still obliged to perform an error analysis. Preliminary efforts suggest an uncertainty in the calculated (counts per channel) of 10-12%, which includes the uncertainty in the neutron source strength.

Appendix A: TART Input for Typical Blank Run

```
name psblk7 rho(all)=normal, 7-9-86
* typical blank run
box a91 gene g.
zplane   27   6.25000e-01
zplane   28   4.75000e-01
zplane   29   1.16200e-01
zplane   30   7.67000e-02
zplane   31   5.00000e-04
zplane   32  -5.00000e-04
zplane   33  -1.19000e+01
zplane   34  -2.49000e+01
zplane   35  -2.74000e+01
jb    1  -32  31  1
jb    2  -31  30  1
jb    3  -30  29  1
jb    4  -29  28  4
jb    5  -32  29  4  -1
jb    6  32  4  8  -3
jb    7  3  -2  32  -34
jb    8  2  32  -33
jb    9  2  -34  -10  33
jb   10  10  -9  33  -34
jb   11  9  33  -34
jb   12  3  34  -35
jb   13  7  -6  27  -4
jb   14  8  -7  -4  27
jb   15  7  -6  -27
jb   16  8  -7  -27
jb   17  5  27  -28
jb   18  5  -4  6  28
jb   19  6  -5  27
jb   20  6  -27
jb   21  11  27  -3  -35  -8
jb   22  11  -27  -8
jb   23  11  35
jb   24  12  -11  15  -27
jb   25  12  -11  -27  -15
jb   26  12  -11  27  -17
jb   27  12  -11  17  -16  27
jb   28  12  -11  16  27
jb   29  13  -12  16  27
jb   30  13  -12  -16  17  27
jb   31  13  -12  -17  27
jb   32  13  -12  15  -27
jb   33  14  -13  15  -27
jb   34  14  -13  -15  -27
jb   35  14  -13  -17  27
jb   36  14  -13  17  -16  27
jb   37  14  -13  16  27
jb   38  13  -12  -27  -15
jb   39  -14
surf    1   1.03100e+00   0.   0.   0.   0.   1.e+00   1.e+00
surf    2   0.  -4.76000e-03   1.11890e+01   0.   0.   1.e+00   1.e+00
surf    3   0.  -4.76000e-03   1.19300e+01   0.   0.   1.e+00   1.e+00
surf    4   2.86000e+00   0.   0.   0.   0.   1.e+00   1.e+00
surf    5   2.86100e+00   0.   0.   0.   0.   1.e+00   1.e+00
surf    6   8.00000e+00   1.00000e+00   0.   0.   0.   1.e+00   1.e+00
surf    7   8.00100e+00   1.00000e+00   0.   0.   0.   1.e+00   1.e+00
surf    8   1.25800e+01   1.00000e+00   0.   0.   0.   1.e+00   1.e+00
surf    9   6.30000e-01   0.   0.   0.   0.   1.e+00   1.e+00
```

Appendix A: TART Input (Continued)

```
surf  10  7.50000e-01  0.  0.  0.  0.  1.e+00  1.e+00
surf  11  8.79000e+02  1.00000e+00  0.  0.  0.  1.e+00  1.e+00
surf  12  8.79010e+02  1.00000e+00  0.  0.  0.  1.e+00  1.e+00
surf  13  9.82500e+02  1.00000e+00  0.  0.  0.  1.e+00  1.e+00
surf  14  9.82510e+02  1.00000e+00  0.  0.  0.  1.e+00  1.e+00
surf  15  0. -3.33333e-01  0.  0.  0.  1.e+00  1.e+00
surf  16  0. -1.42039e+00  0.  0.  0.  1.e+00  1.e+00
surf  17  0. -7.54876e+00  0.  0.  0.  1.e+00  1.e+00
matl  1 1.6000e+00 5.0000e-01  1003 5.0000e-01 22000
matl  2 1.8800e+01 1.0000e+00 74000
matl  3 8.0000e+00 4.5000e-01 26000 3.2000e-01 29000 8.0000e-02  8016   &
 2.0000e-02 13027 6.0000e-02  6012 1.3000e-01  1001
matl  4 3.9000e+00 5.0000e-01 13027 3.0000e-01  1001 2.0000e-01  6012
matl  5 2.7000e+00 1.0000e+00 13027
matl  6 1.2880e-03 7.8850e-01  7014 2.1150e-01  8016
matl  7 8.0000e+00 5.0000e-01 13027 5.0000e-01 29000
matl  8 7.9000e+00 6.8600e-01 26000 8.4000e-02 28000 2.0000e-02 14000   &
 1.0000e-02 25055 2.0000e-01 24000
matl  9 1.8340e+00 1.0000e+00  4009
matz  0  39
matz  1  1
matz  2  2
matz  3  3
matz  4  5
matz  5  7  10
matz  6  4  6  8  9  11  17  18  19  20  21  22  23  24  25  26  27  28  29
matz  6  30  31  32  33  34  35  36  37  38
matz 6 13 14 15 16
matz  7  12
c    matz  9  13  14  15  16
sentl  1 0  2 20  3 40000  5 3  12 2  21 20  22 1  33 3
sentl  6  2.00000e+00  7 -1.00000e+00  8 -1.00000e-01  9 -1.00000e-04
sentl  10  5.00000e-05  13  5.00000e-01  14  1.00000e-04  15  2.00000e+01
sentl  16  1.60000e+01
eangl  1  1.00000e+00  1.00000e+00  9.96000e-01  9.39690e-01
eangl  3  9.84550e-01  7.66040e-01  9.67200e-01  5.00000e-01
eangl  5  9.46220e-01  1.73650e-01  9.24278e-01 -1.73650e-01
eangl  7  9.04006e-01 -5.00000e-01  8.87732e-01 -7.66040e-01
eangl  9  8.77232e-01 -9.39690e-01  8.73608e-01 -1.00000e+00
enerangl  1  1.51060e+01  1.00000e+00  1.50450e+01  9.39690e-01
enerangl  3  1.48690e+01  7.66040e-01  1.46050e+01  5.00000e-01
enerangl  5  1.42860e+01  1.73650e-01  1.39550e+01 -1.73650e-01
enerangl  7  1.36510e+01 -5.00000e-01  1.35070e+01 -7.66040e-01
enerangl  9  1.32510e+01 -9.39690e-01  1.31970e+01 -1.00000e+00
source2  1  0.  6.00000e-01  0.  0.  0.  0.
centim  80.0
ltype  0  1  2  3  4  5  6  7  8  9  10  11  12  13  14  15  16  17
ltype  0  18  19  20  21  22  23  25  26  27  28  29  30  31  32  33  34  35
ltype  0  36  37  38  39
ltype  12  24
ltypeg 12 24
timspec  1  0.  0.  1.26000e+01  3.17400e-01
timspec  3  3.78000e+01  7.93500e-01  5.67000e+01  9.52200e-01
timspec  5  9.45000e+01  1.11100e+00  2.39400e+02  1.27000e+00
timspec  7  3.49090e+03  1.42800e+00  3.70825e+04  1.58700e+00
timspec  9  1.54228e+05  1.74600e+00  1.26963e+05  1.90400e+00
timspec  11  2.45054e+04  2.06300e+00  7.46060e+03  2.22200e+00
timspec  13  3.88780e+03  2.38100e+00  2.15500e+03  2.53900e+00
timspec  15  1.17200e+03  2.69800e+00  6.61600e+02  3.01500e+00
timspec  17  3.52900e+02  3.49100e+00  1.57500e+02  4.28500e+00

timspec  19  7.56000e+01  5.07800e+00  3.15000e+01  5.87200e+00
timspec  21  6.30000e+00  6.66500e+00  0.  7.45900e+00
end
```

Appendix A (Continued): SANDYL Input;

Gamma-Ray Spectrum from TART Blank Run

```
BOX A91 HANDYL GENE GOLDBERG                                                    Ø
  SANDYL BLKPS1 NE213 DET., GAMMA SPECTRUM F'M TART PSBLK7 7-1Ø-86              1
  1Ø  13   4   8          2Ø   2ØØØØ   2       1                              2
   Ø                       7                                          5       3
        .ØØ1         9.9Ø                                                    3D
   2  -2 -11  -1  12   4                                                     6   1
   4  -3  -1  -2   3   1                                                     6   2
   4  -3  -1  -2  12   4  -2   1                                            6   3
   5  -4  -2  -3  12   4                                                     6   4
   6  -5  -4  -4  12   4                                                     6   5
   7  -6  -5  -5  12   4                                                     6   6
  1Ø  -7  -6  -6   8   2                                                     6   7
  1Ø  -7  -6  -6   9   3  -7   2                                            6   8
  1Ø  -7  -6  -6  12   4  -8   3                                            6   9
  13  -8  -7  -7  12   4                                                     6  1Ø
  11  -1                                                                     6  11
 -12   4                                                                     6  12
 -13  -8                                                                     6  13
                        Ø.       2.694      -17.ØØØ          Ø.        1.Ø   7
       -33.Ø                      .ØØ1          Ø.                          8
       -.ØØ1                                                                9
          Ø.          Ø.         Ø.          Ø.        .635                 1Ø
          Ø.          Ø.         Ø.          Ø.       2.457                 1Ø
          Ø.          Ø.         Ø.          Ø.       2.53Ø                 1Ø
          Ø.          Ø.         Ø.          Ø.       2.695                 1Ø
        -2Ø.      -15.Ø13       -15.          Ø.        .ØØ38       .216    11
       5.278        5.918                                                    11
  1   1                                                                      12   1
  1   1                                                                      11   1
  1   1                                                                      12   3
  1   1                                                                      12   4
  5   1                                                                      12   5
  2   1                                                                      12   6
  3   1                                                                      12   7
  1   1                                                                      12   8
  2   1                                                                      12   9
  4   1                                                                      12  1Ø
  Ø.          2.3ØØØE-Ø1  3.1ØØØE-Ø1  3.8ØØØE-Ø1  4.6ØØØE-Ø1  5.3ØØØE-Ø1      16
  6.ØØØØE-Ø1  6.9ØØØE-Ø1  7.9ØØØE-Ø1  8.4ØØØE-Ø1  9.ØØØØE-Ø1  1.Ø1ØØE+ØØ      16
  1.Ø6ØØE+ØØ  1.16ØØE+ØØ  1.26ØØE+ØØ  1.36ØØE+ØØ  1.45ØØE+ØØ  1.59ØØE+ØØ      16
  1.7ØØØE+ØØ  1.82ØØE+ØØ  1.91ØØE+ØØ  2.Ø4ØØE+ØØ  2.16ØØE+ØØ  2.27ØØE+ØØ      16
  2.46ØØE+ØØ  2.67ØØE+ØØ  2.95ØØE+ØØ  3.12ØØE+ØØ  3.49ØØE+ØØ  3.92ØØE+ØØ      16
  4.8ØØØE+ØØ  6.66ØØE+ØØ  9.95ØØE+ØØ                                         16
  1   2      .ØØ129        .8  7        .2  8                                 18
  2   1        2.71       1.Ø 13                                             18
  3   2       Ø.884        .55  1       .45  6                               18
  4   2         2.2        .667  8      .333 14                               18
  5   2         1.Ø        .667  1      .333  6                               18
```

5-7-86

FIGURE 1

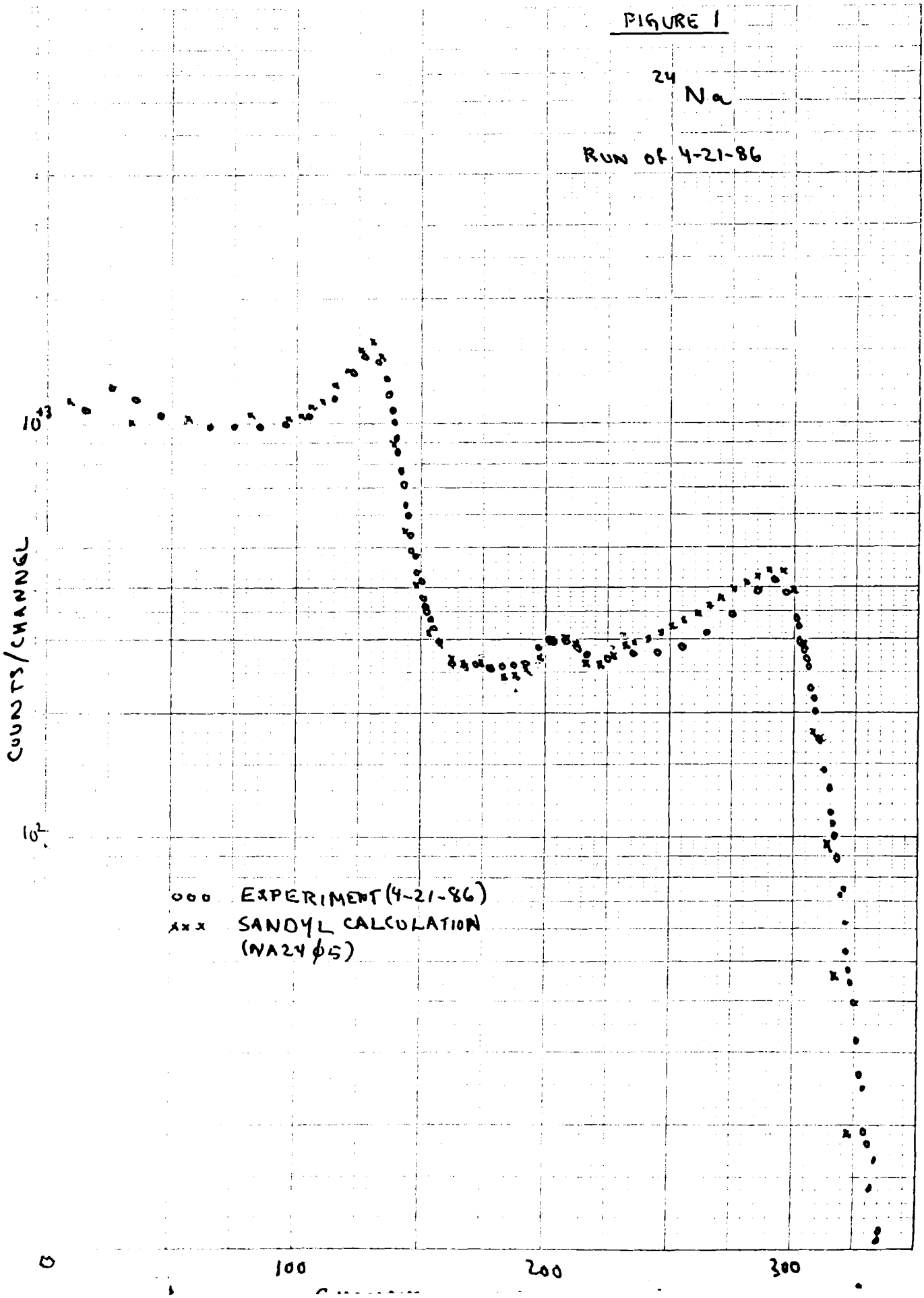

5-12-86

FIGURE 2

^{22}Na

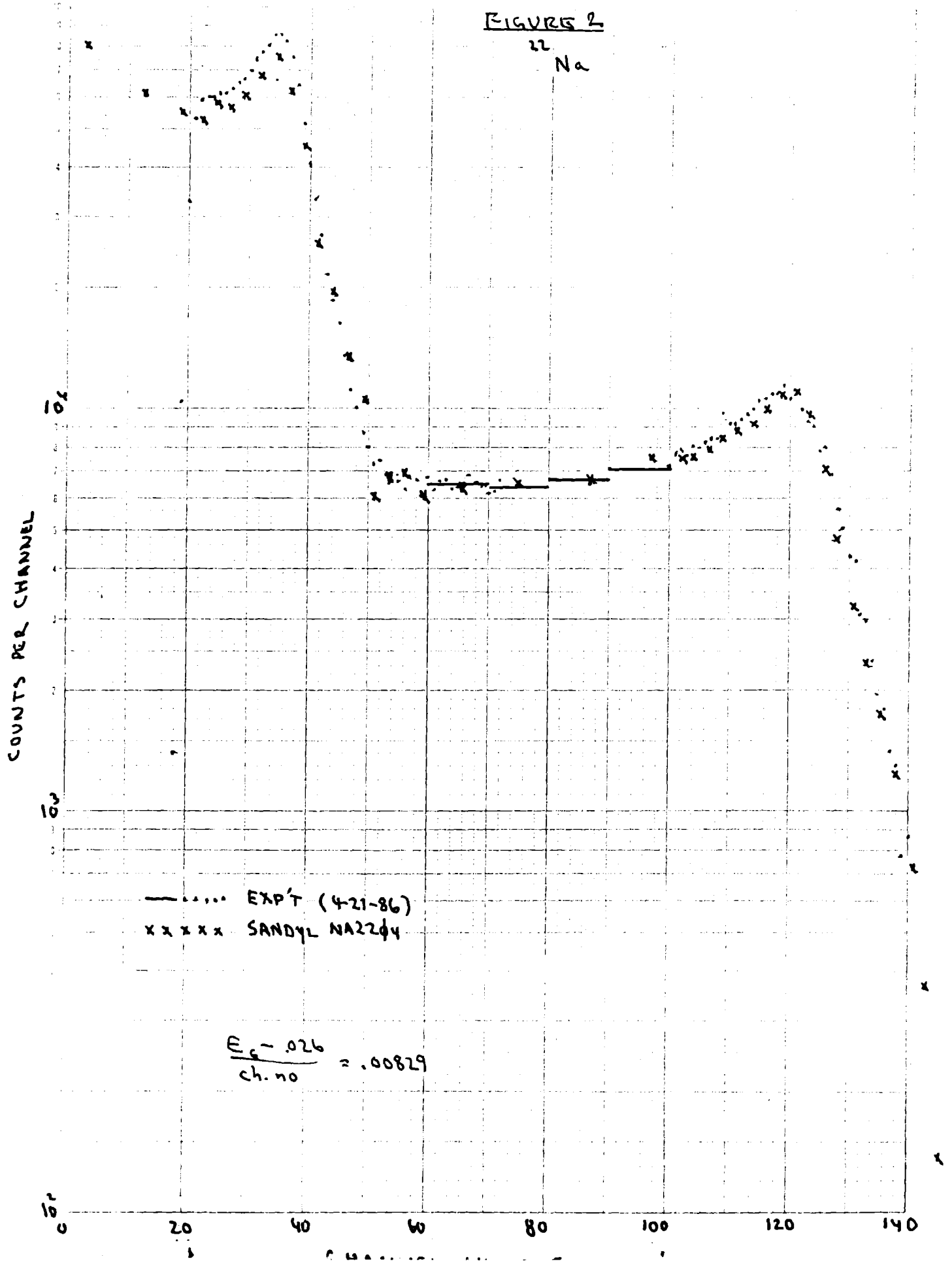

5-12-86

FIGURE 3. ^{137}Cs

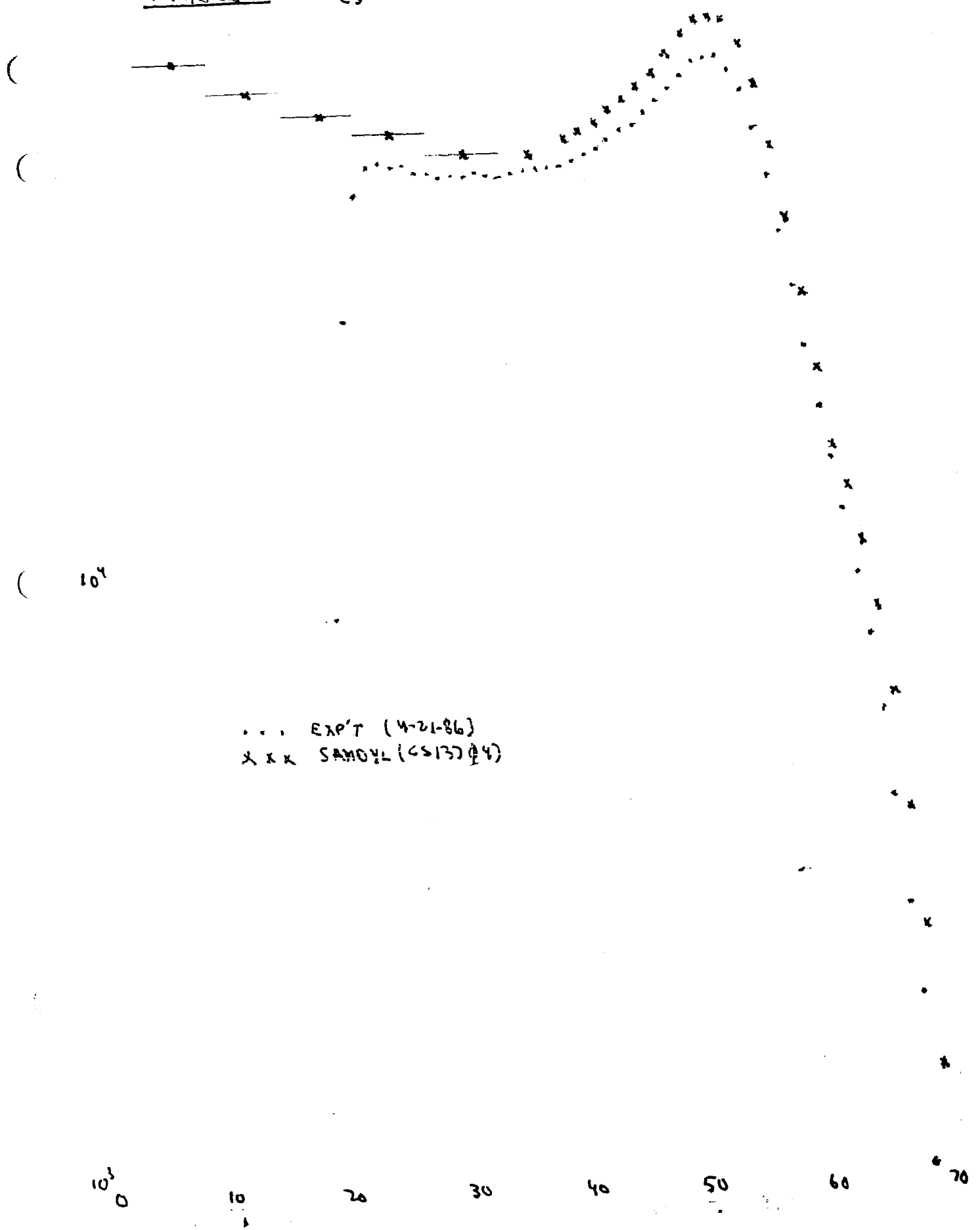

5-12-86

FIGURE 4

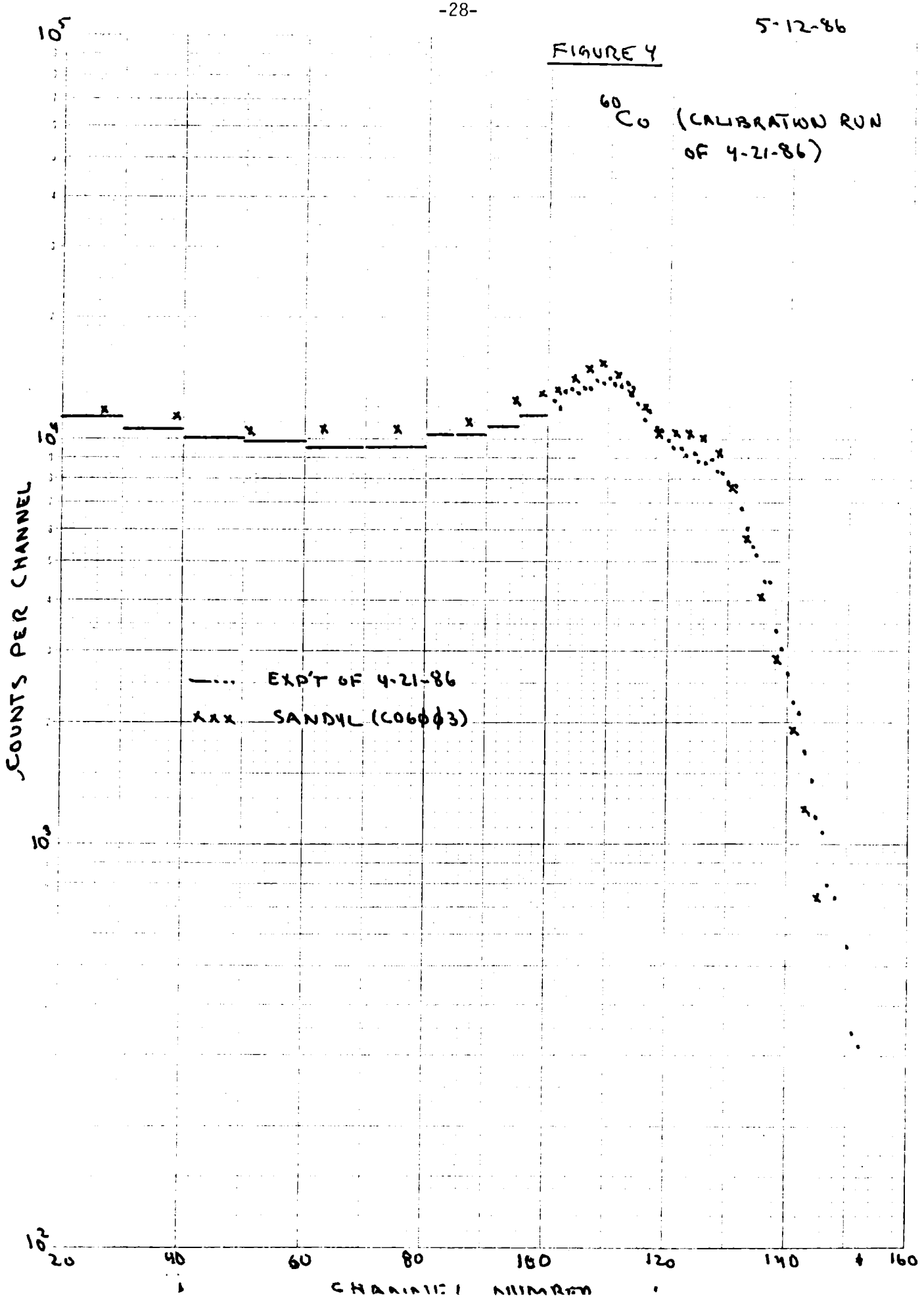

8-19-86

FIGURE 5A

$E_{ELECTRON}$ VS CHANNEL NO.

NE-213 DETECTOR

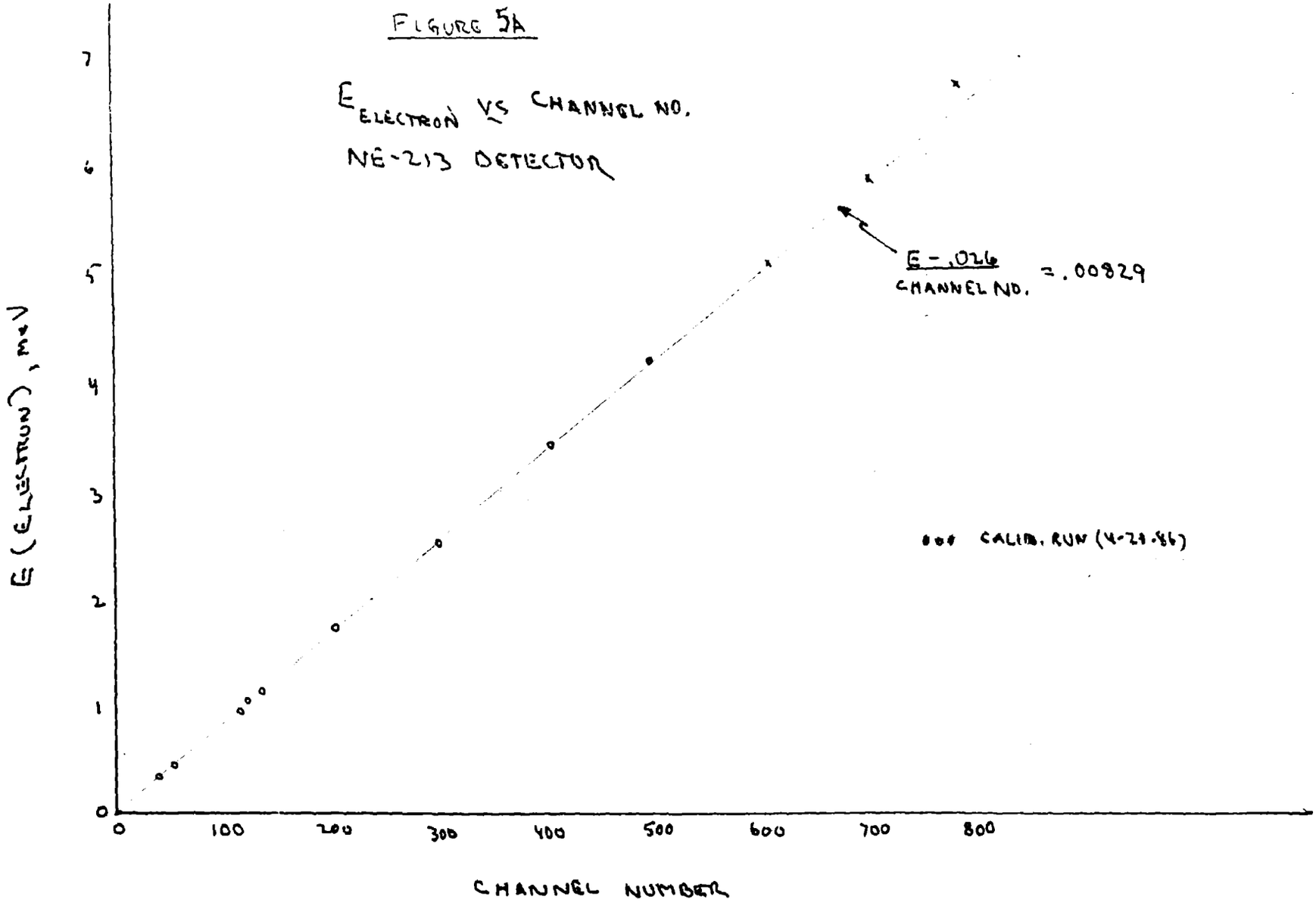

8-19-86

FIGURE 5B

E (ELECTRON) VS CHANNEL NO.

(NE213 DETECTOR)

$\frac{E - .026}{\text{CHANNEL NO.}} = .008285$

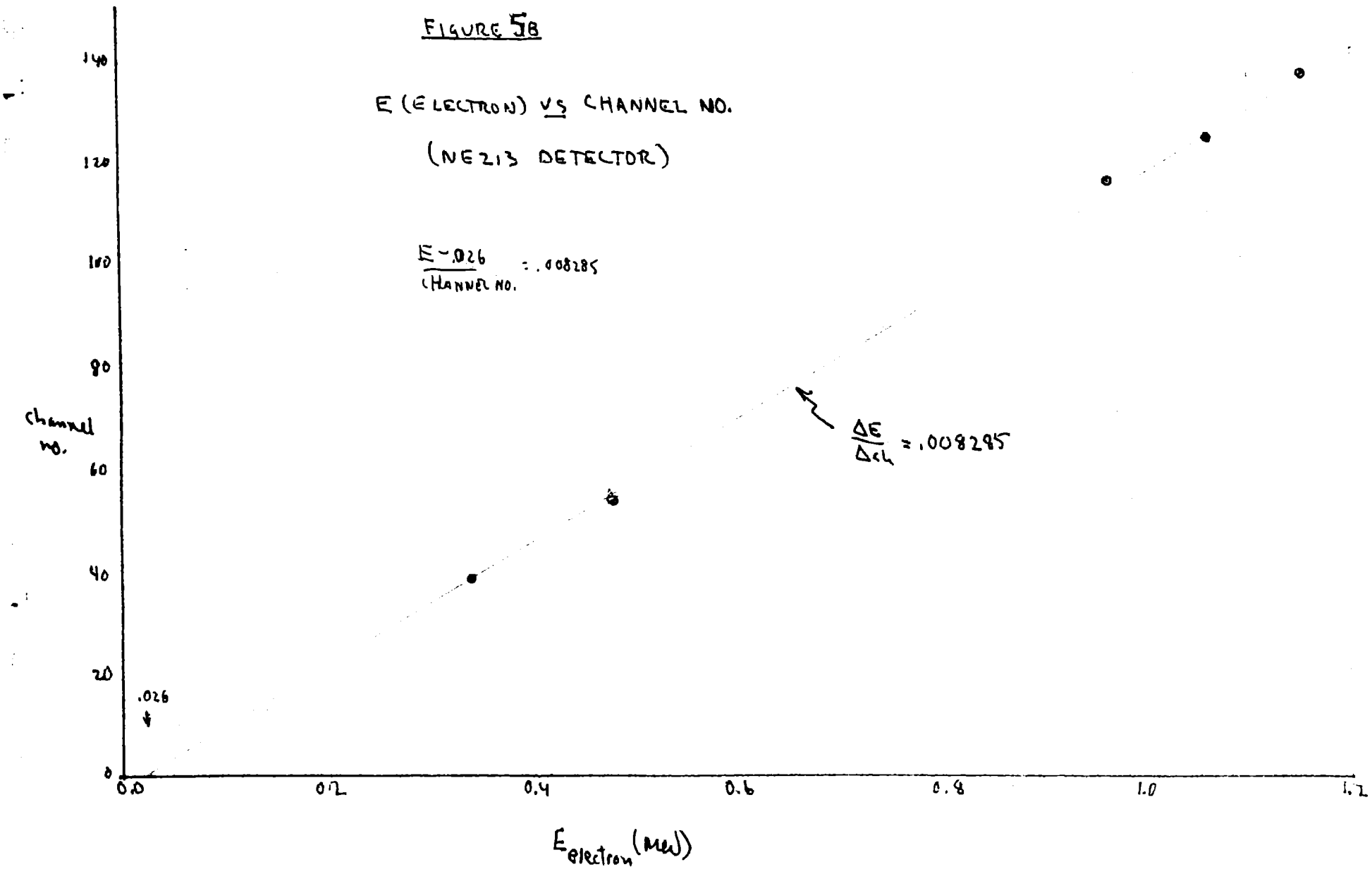

5-22-86

FIGURE 6

^{22}Na

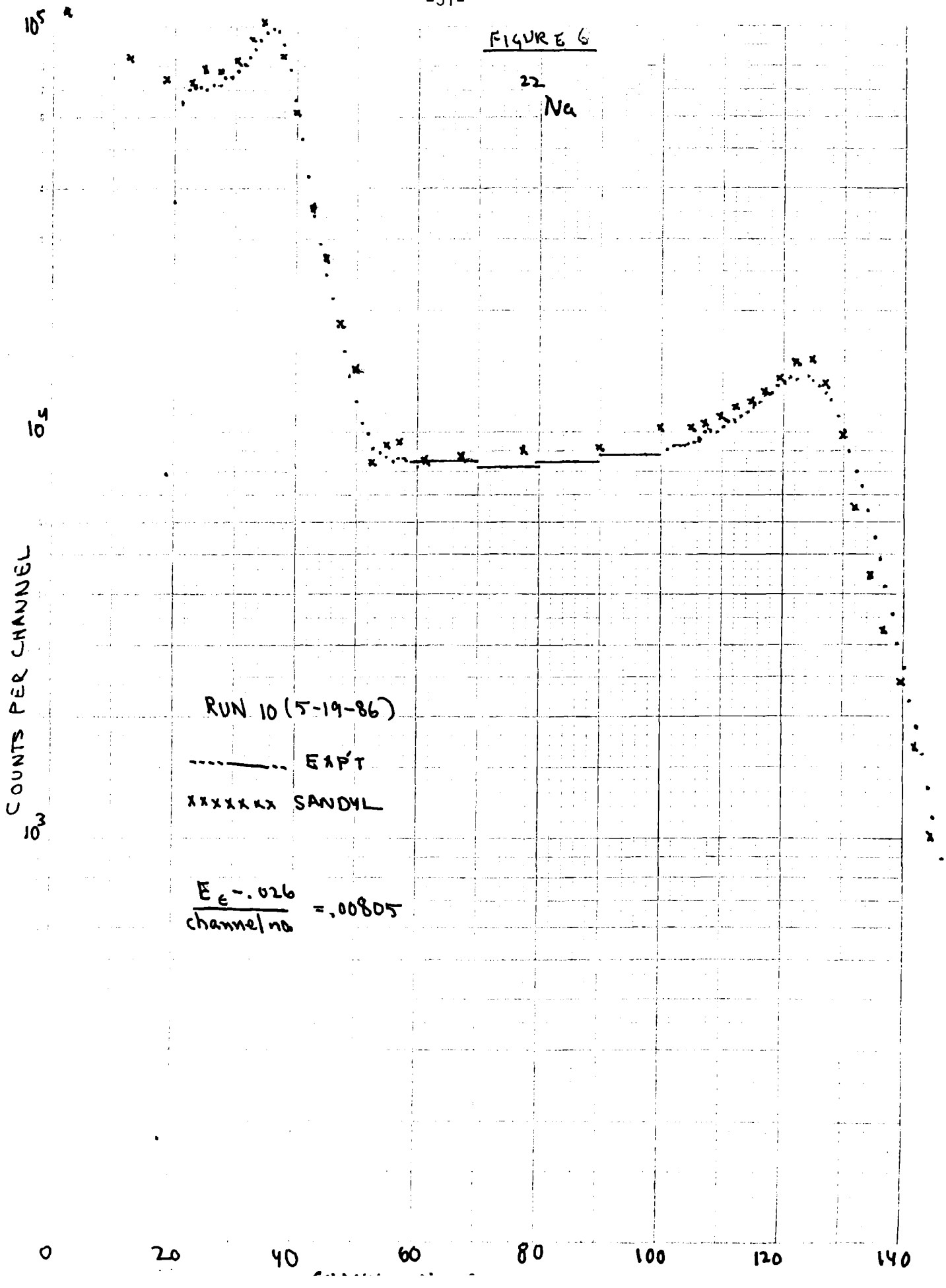

8-25-86

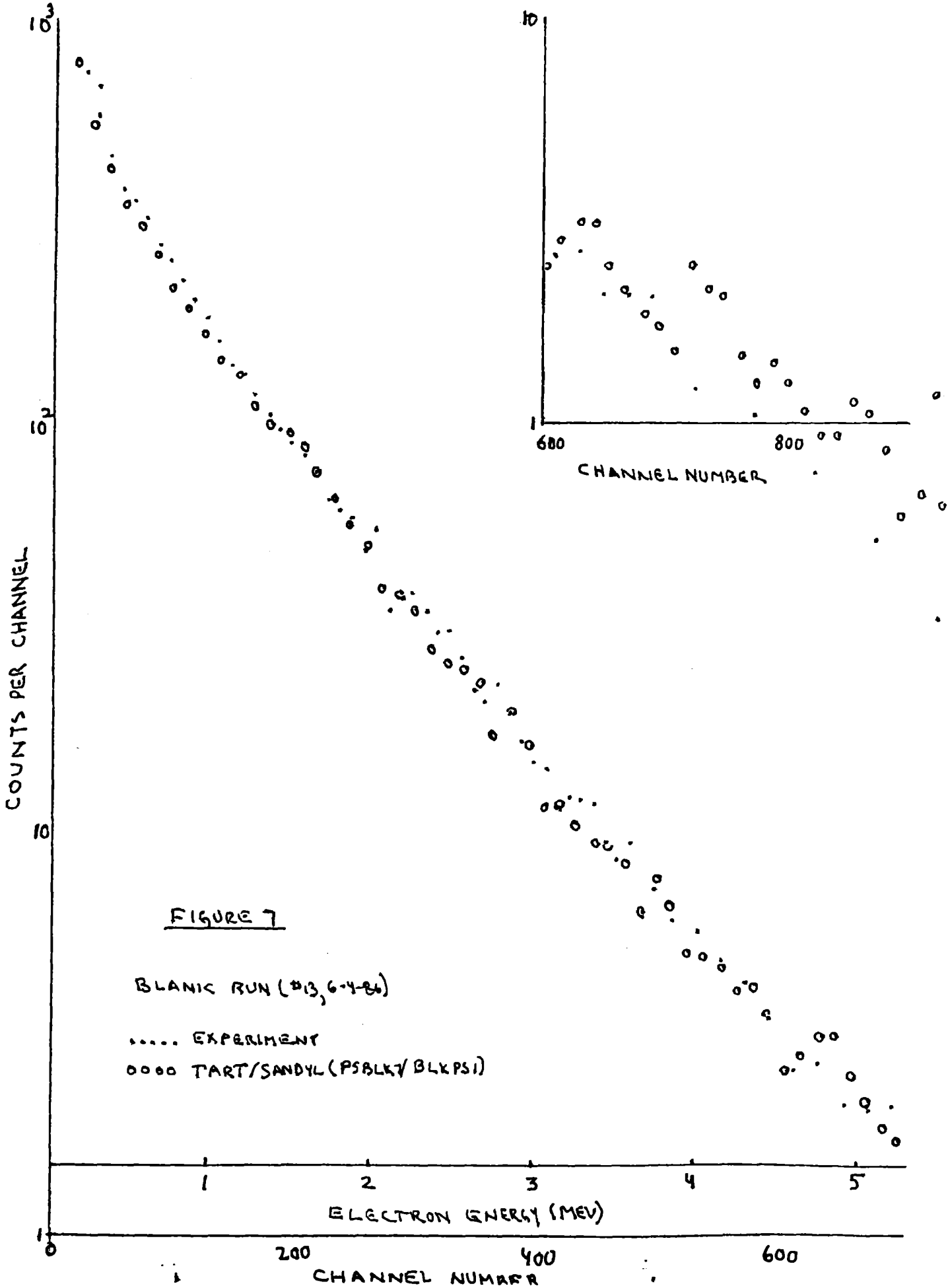

FIGURE 7

8-29-86

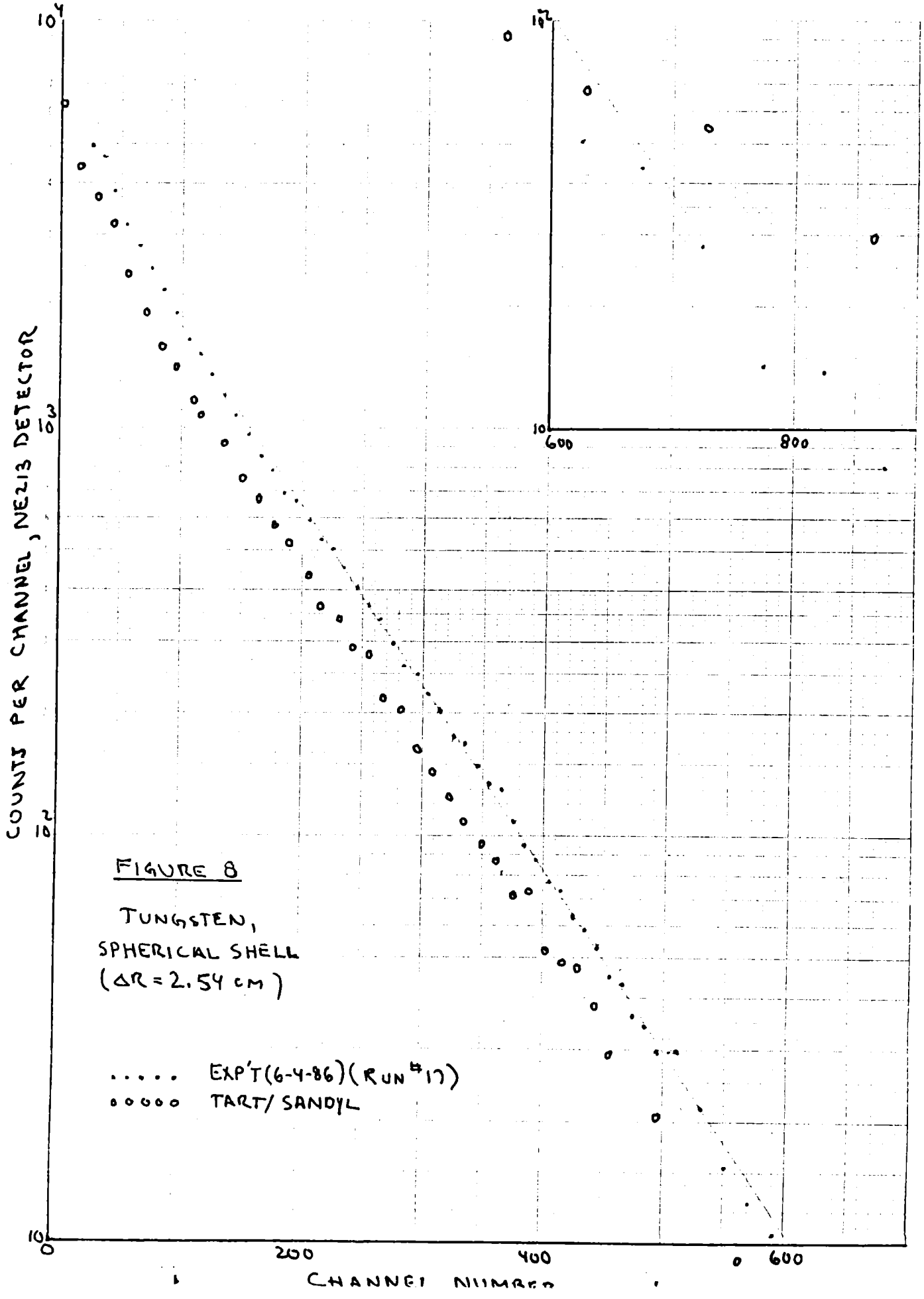

FIGURE 8

TUNGSTEN, SPHERICAL SHELL ($\Delta R = 2.54$ cm)

..... EXP'T (6-4-86) (RUN #17)

ooooo TART/SANDYL

9-2-86

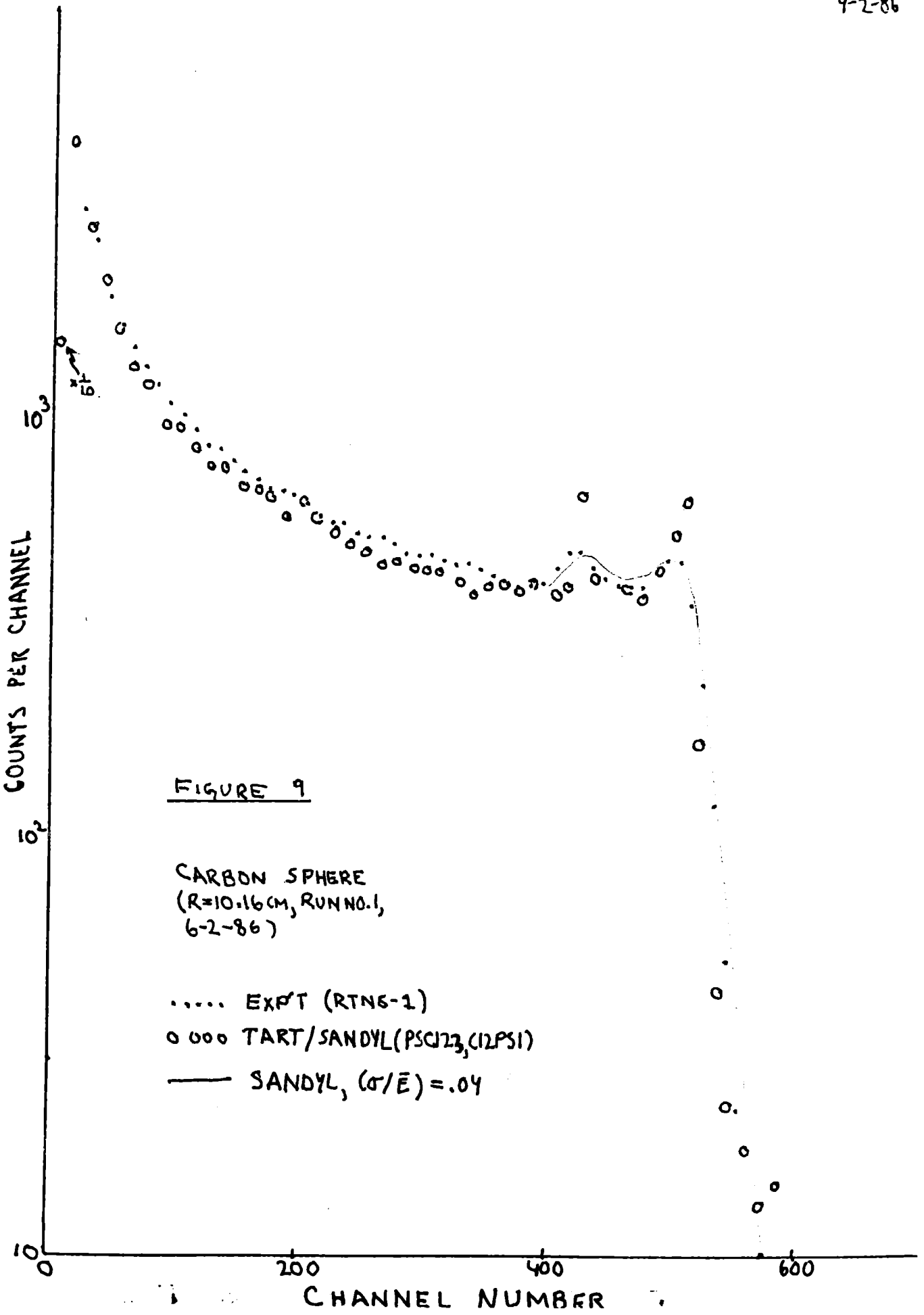

FIGURE 9

CARBON SPHERE
(R=10.16 CM, RUN NO. 1,
6-2-86)

..... EXPT (RTN6-1)

o ooo TART/SANDYL (PSC123, C12PS1)

—— SANDYL, $(\sigma/\bar{E}) = .04$

9-2-86

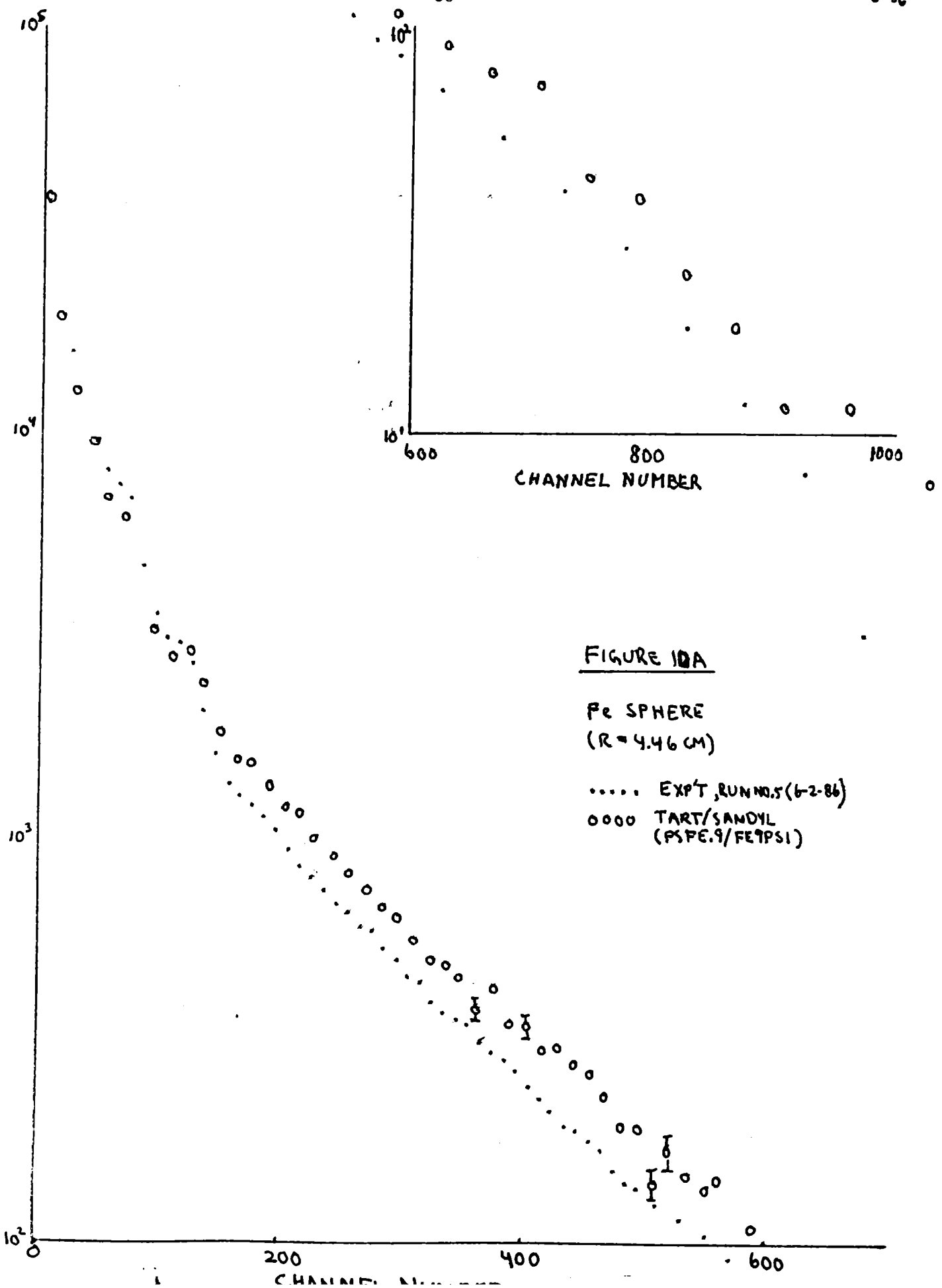

FIGURE 10A

Fe SPHERE
(R = 4.46 CM)

..... EXP'T, RUN NO. 5 (6-2-86)

oooo TART/SANDYL
(PSPE.9/FE9PS1)

9-2-86

FIGURE 10 B

FE SPHERE
(R = 4.46 CM)
(REDUCED GAIN IN P.H.A.)

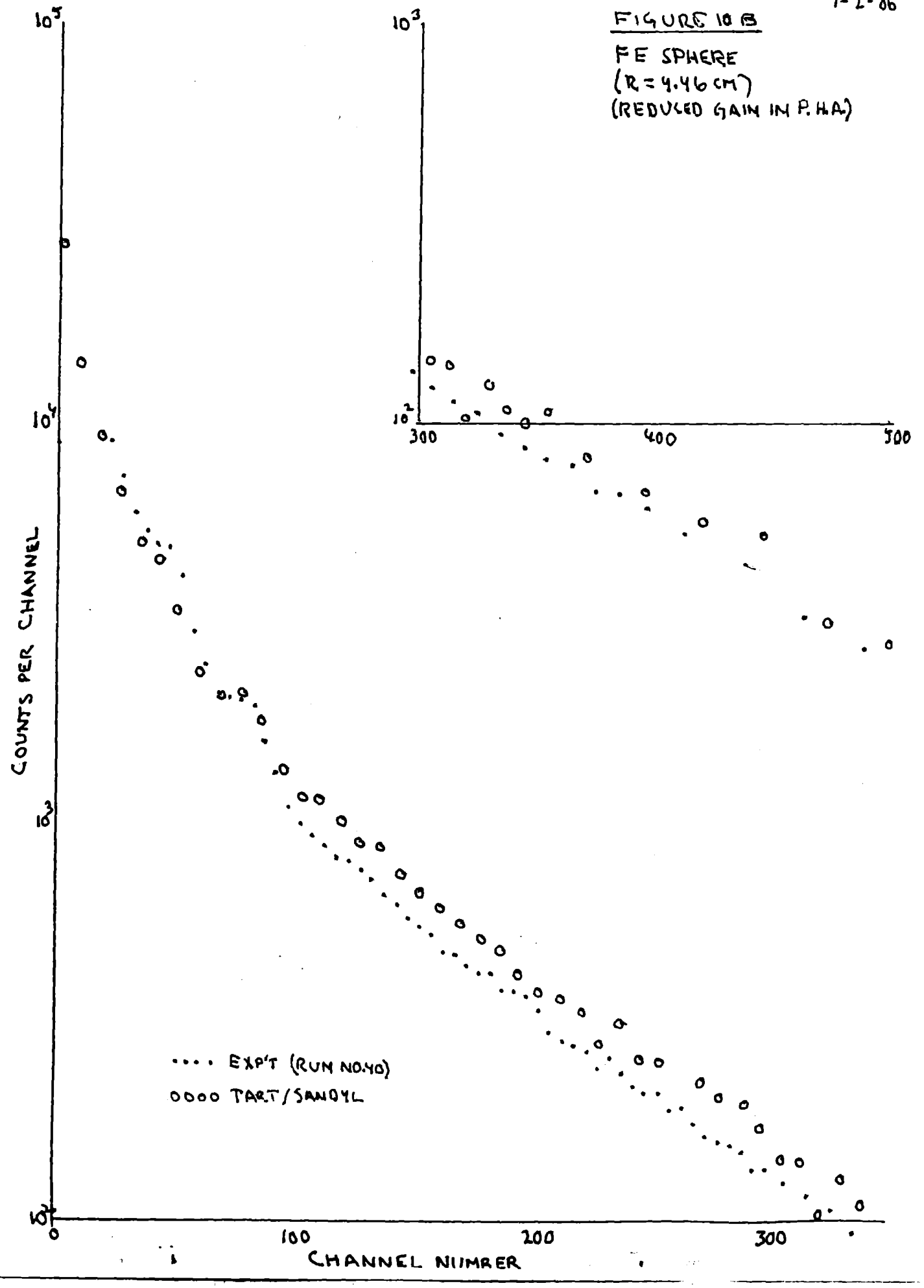

9-4-86

FIGURE II

EMPTY GLASS VESSEL
(RUN NOS, 6-3-86)

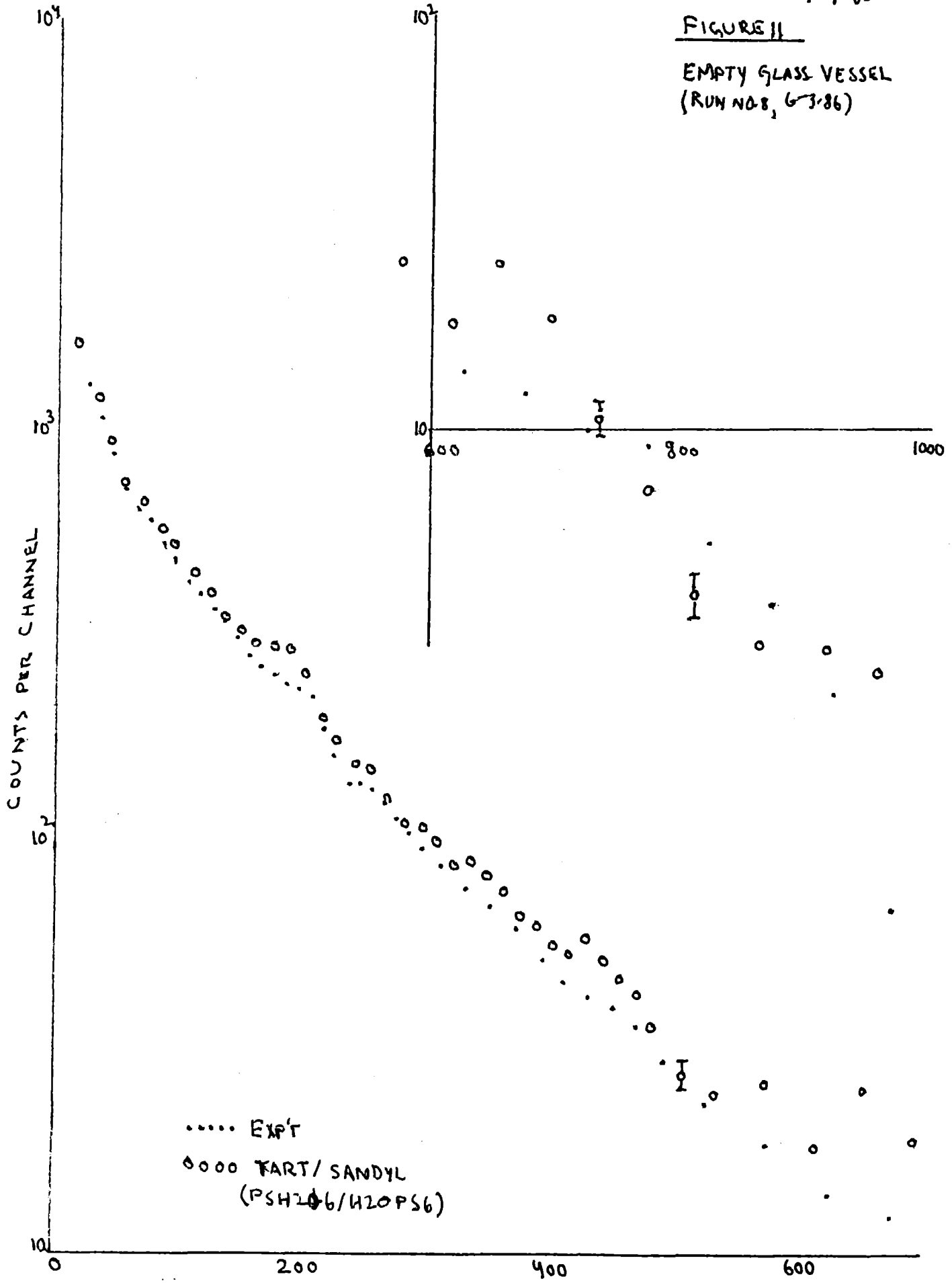

9-4-86

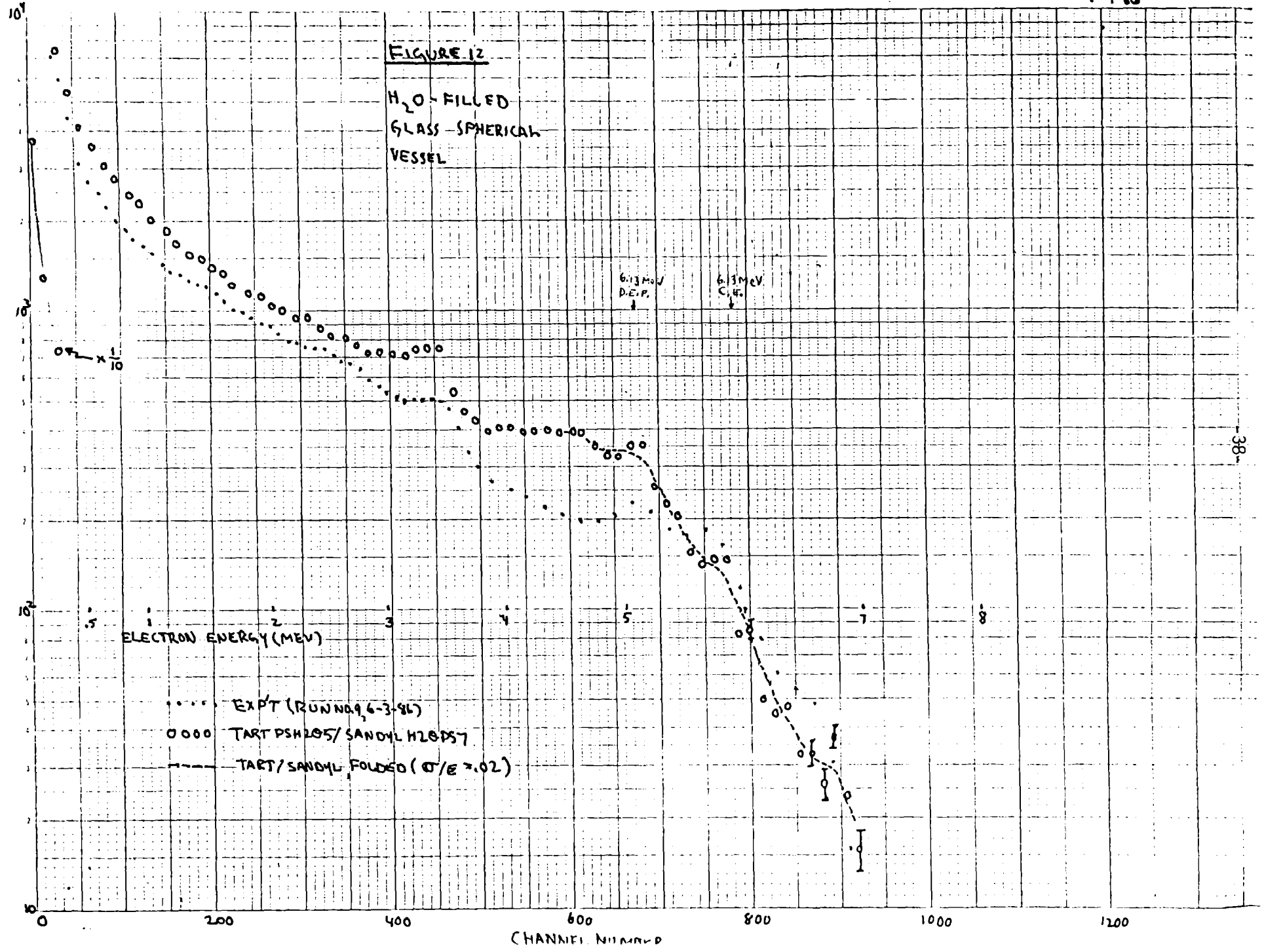
FIGURE 12
H_2O - FILLED GLASS SPHERICAL VESSEL
6.13 MeV D.E.P.
6.13 MeV C_{14}
$\times \frac{1}{10}$
ELECTRON ENERGY (MEV)
.5
1
2
3
4
5
7
8
EXPT (RUN NO. 9, 6-3-86)
TART PSH205/ SANDYL H20DS7
TART/ SANDYL FOLDED (σ/ε = .02)
0
200
400
600
800
1000
1200
CHANNEL NUMBER

9-V-86

FIGURE 13

^{238}U SPHERE
(R = 3.63 CM.)

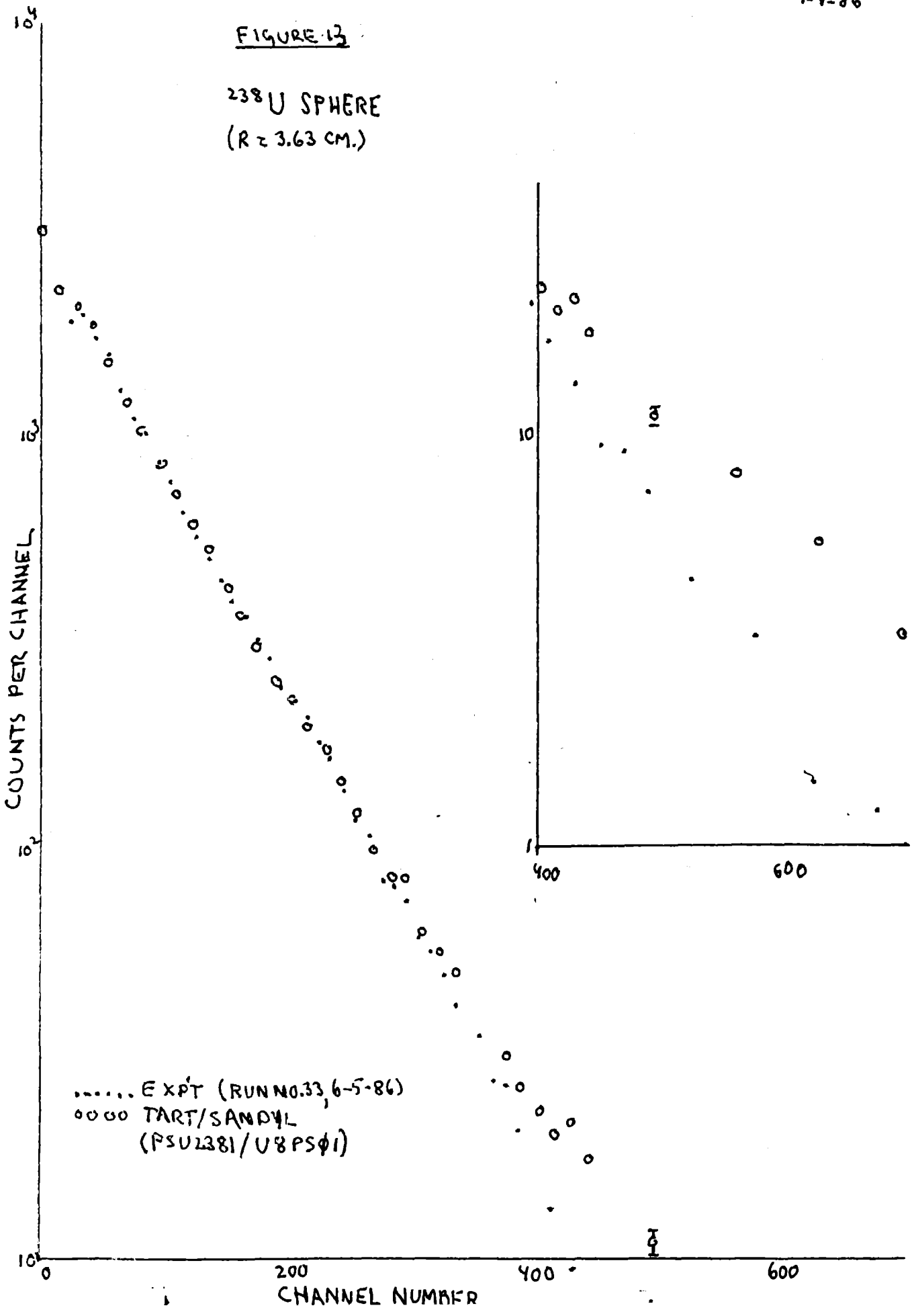

9-4-86

FIGURE 14

^{232}TH SPHERE
(R=5.757 CM.)

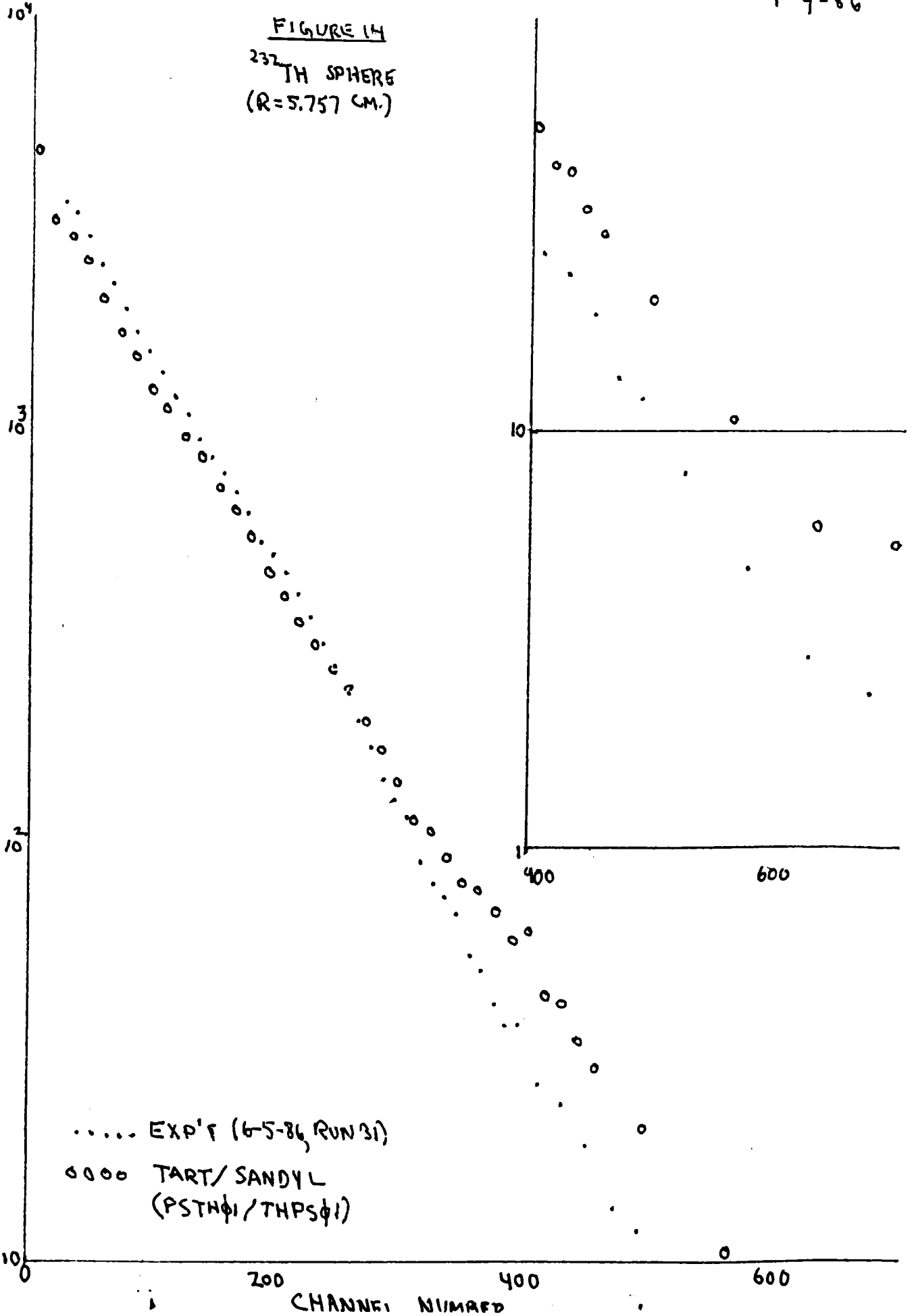

1-3-86

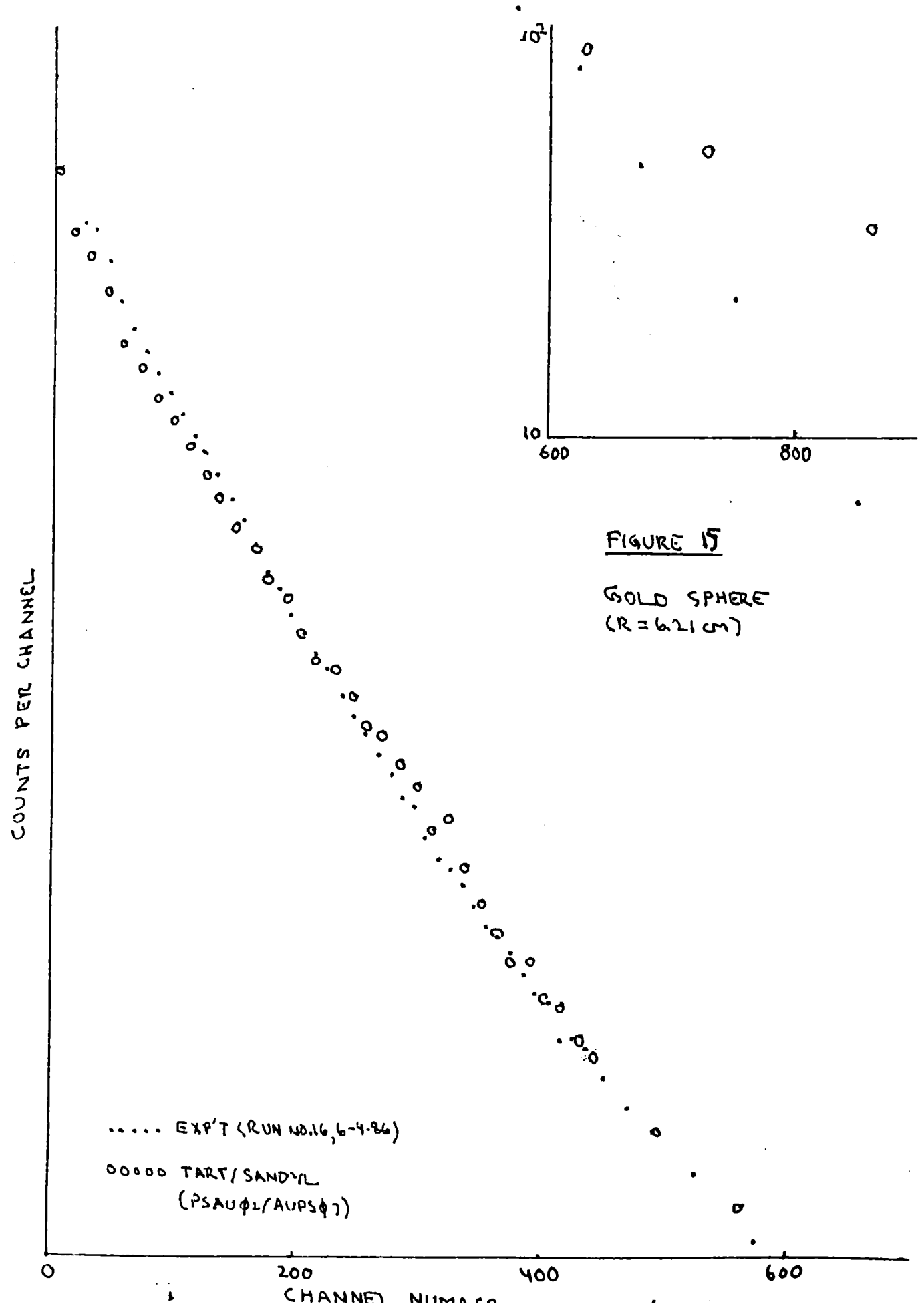

FIGURE 15

GOLD SPHERE
(R = 6.21 cm)

9-3-86

FIGURE 16

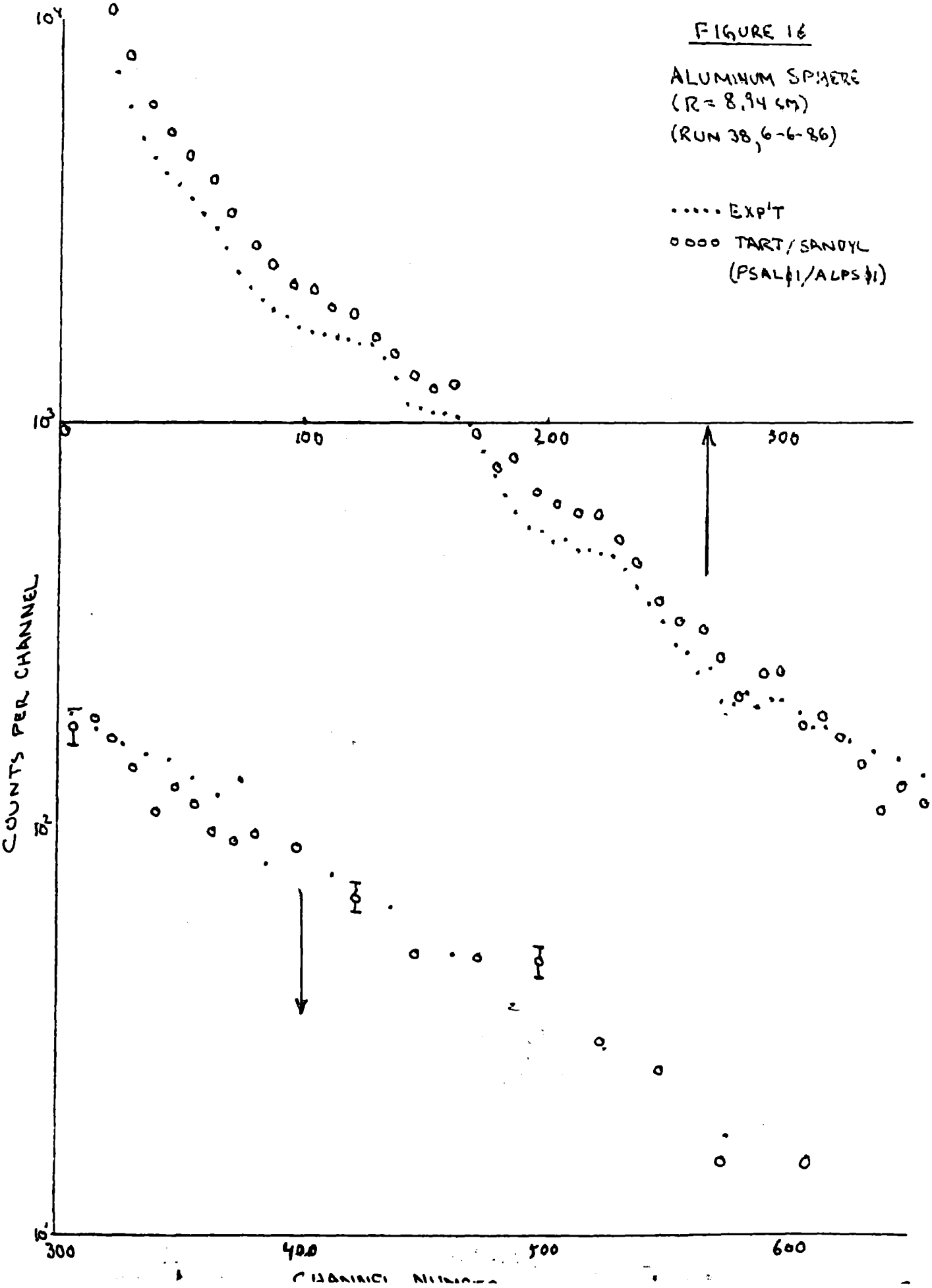

9-15-86

FIGURE 17

C_u SPHERE
(R = 4.00 cm)

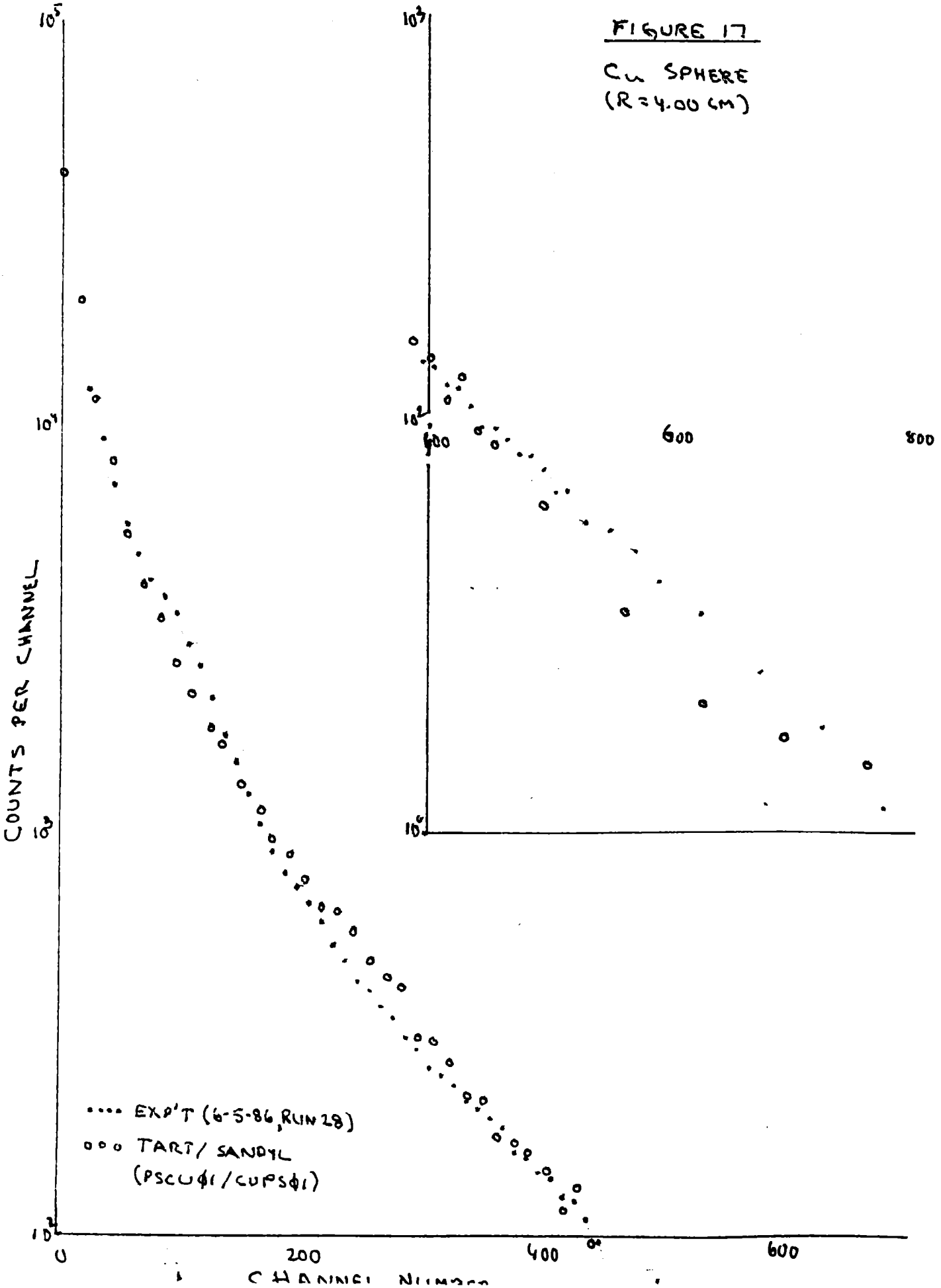

9-15-86

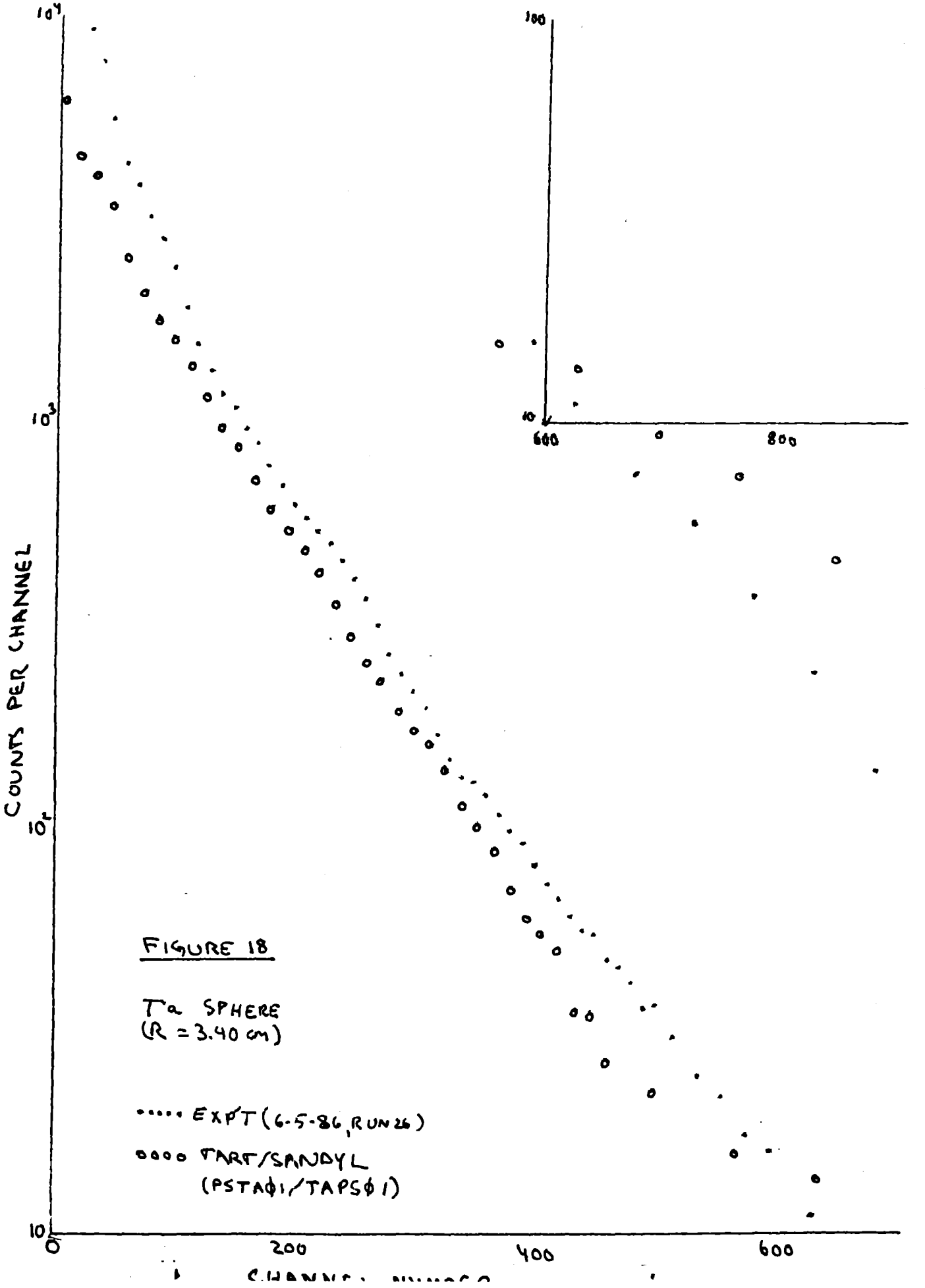

FIGURE 18

Ta SPHERE
(R = 3.40 cm)

..... EXPT (6-5-86, RUN 26)

oooo TART/SANDYL
(PSTAΦ1/TAPSΦ1)